AIMS Mathematics, 10(1): 1248–1299.
DOI: 10.3934/math.2025059
Received: 18 November 2024
Revised: 24 December 2024
Accepted: 02 January 2025
Published: 21 January 2025

https://www.aimspress.com/journal/Math

Research article

Dynamics analysis of spatiotemporal discrete predator-prey model based on coupled map lattices

Wei Li[1], **Qingkai Xu**[1], **Xingjian Wang**[2,*] **and Chunrui Zhang**[1]

[1] College of Mathematics, Northeast Forestry University, Harbin 150040, China
[2] College of Computer and Control Engineering, Northeast Forestry University, Harbin 150040, China

* **Correspondence:** Email: jianxingwang@126.com.

Abstract: In this paper, we explore the dynamic properties of discrete predator-prey models with diffusion on a coupled mapping lattice. We conducted a stability analysis of the equilibrium points, provided the normal form of the Neimark-Sacker and Flip bifurcations, and explored a range of Turing instabilities that emerged in the system upon the introduction of diffusion. Our numerical simulations aligned with the theoretical derivations, incorporating the computation of the maximum Lyapunov exponent to validate obtained bifurcation diagrams and elucidated the system's progression from bifurcations to chaos. By adjusting the self-diffusion and cross-diffusion coefficients, we simulated the shifts between different Turing instabilities. These findings highlight the complex dynamic behavior of discrete predator-prey models and provide valuable insights for biological population conservation strategies.

Keywords: predator-prey model; coupled map lattices; Neimark-Sacker bifurcation; Flip bifurcation; Turing instability; chaos
Mathematics Subject Classification: 34C23, 37N25

1. Introduction

In recent years, research in the field of biological modeling has flourished, leading to distinctive research outcomes by adopting diverse methods to address the characteristics of biological populations [1, 2]. Different biological populations impose distinct requirements on the selection of research methods due to their unique life cycles, reproduction patterns, and ecological adaptations. For populations with short life cycles, well-defined reproductive cycles, or non-overlapping generations, discrete biological models exhibit higher accuracy in describing dynamic changes. In scientific research, biological data are often recorded and collected at a series of discrete time points. Discrete

biological models, leveraging their advantages, are more effective in handling nonlinear relationships based on discrete time points. By flexibly adjusting the model parameters, discrete biological models can simulate the interactions between biological populations in different contexts.

Furthermore, discrete models exhibit a wide range of dynamic properties. Apart from the common phenomena of convergence, oscillation, and chaos, discrete models can also unveil more intricate dynamic behaviors, such as period-doubling bifurcations and strange attractors. These complex dynamic phenomena are often challenging to directly observe and analyze in continuous models, but they can be clearly and intuitively demonstrated and thoroughly analyzed in discrete models. An increasing number of scholars have delved into the study of discrete biological models [3–7], which enable a more comprehensive description of the behaviors and characteristics of biological populations by incorporating additional biological parameters and more intricate interactions. This advancement not only propels theoretical development in the field of biology but also offers robust support for practical applications.

A discretized reaction-diffusion system in both space and time can be interpreted as a coupled map lattice (CML) model. Through the utilization of the coupled map lattice model, researchers have extensively explored the dynamic variations of biological populations within ecosystems [8–10], encompassing crucial processes like species migration, competition, and coexistence. This exploration not only enhances our understanding of ecosystem stability and sustainability but also establishes a robust scientific foundation for ecological conservation and management. In comparison to traditional continuous models, the coupled map lattice model demonstrates notable advantages in addressing intricate spatio-temporal dynamics and nonlinear interactions. By segmenting the system into discrete patches and meticulously considering inter-patch interactions, we can intuitively and clearly unveil the spatial structure and dynamics of the predation system.

The predator-prey model, as a significant tool in the realms of ecology and mathematics, has undergone continuous refinement and advancement since the introduction of the Lotka-Volterra model in the early 20th century [11, 12]. It has evolved into a crucial instrument for studying species relationships and dynamics within ecosystems. Researchers have developed diverse forms of predator-prey models based on varying assumptions and conditions. These models consider factors such as species growth rate, predation rate, and mortality rate, among others, to depict interactions among biological populations. To better capture the complexity of ecosystems, nonlinear relationships and different functional response functions have been incorporated into the models [13–17]. The comprehensive exploration of predator-prey modeling has unveiled the intricacies of species interactions and showcased diverse interdisciplinary applications in fields such as economics and sociology.

In the predator-prey model of ecology, herd behavior is characterized by the tendency of prey or predators to gather and form groups in response to imminent predation threats. For example, on the African savannah, antelope herds migrate collectively to safer areas when confronted with predators like lions. This migratory behavior serves to safeguard the herd from predators. Moreover, during migration, antelope herds cooperate to address environmental challenges. Consequently, a more sophisticated social model was proposed in reference [18] to depict the behavior of large herbivore populations on the savannah,

$$\begin{cases} \frac{du}{dt} = ru(1-u) - \sqrt{u}v, \\ \frac{dv}{dt} = \beta v\left(-\alpha + \sqrt{u}\right), \end{cases}$$

where $u(t)$ and $v(t)$ denote the prey and predator densities at time t, respectively. α is the mortality rate of the predator in the absence of prey, and β is the rate at which prey is converted to predators.

In this model, individuals within a population exhibit a tendency to aggregate and form large groups, with stronger individuals positioned at the periphery of the group and weaker individuals clustered towards the center. This spatial differentiation leads to successful predation by predators primarily occurring at the boundaries of the group, affecting individuals at the outermost part of the group. When examining this concept through a mathematical lens, the number of individuals at the population boundary is proportional to the perimeter of the occupied area, which, in turn, is proportional to the square root of the area. Given that individuals in the population are distributed in two dimensions, the estimation of the number of individuals at the edge can be derived from the square root of the area. Consequently, when modeling predator attacks on populations, the functional response can be formulated based on the square root of the prey population density.

Indirect effects of predators, such as fear effects, can significantly impact the dynamics of ecosystems. Research indicates that the mere presence of a predation threat can compel prey to alter their behavior and exhibit antipredator responses, such as selecting new habitats, adjusting foraging times, and seeking safer foraging sites. These behavioral changes may result in reduced prey growth, survival, and reproductive rates. To investigate this phenomenon, Wang et al. [19] introduced an expression $f(k, y) = \frac{1}{1+ky}$ to quantify the impact of fear on prey populations, with the level of fear represented by the parameter k. In 2019, Zhang et al. [20] studied a predator-prey system incorporating the fear effect and refuge,

$$\begin{cases} \frac{du}{dt} = \frac{\alpha u}{1+kv} - bu^2 - \frac{\beta(1-m)uv}{1+a(1-m)u}, \\ \frac{dv}{dt} = -rv + \frac{c\beta(1-m)uv}{1+a(1-m)u}, \end{cases}$$

analyzing and numerically exploring the influence of fear effects on the model. Fakhry [21] proposed a predator-prey model with fear effects and population effects.

$$\begin{cases} \frac{du}{dt} = ru(1-u)\left(\frac{1}{1+kv}\right) - \sqrt{u}v, \\ \frac{dv}{dt} = -\alpha v + \beta\sqrt{u}v. \end{cases}$$

In natural ecosystems, interactions and dispersal among biological populations are widespread, with the spatial distribution and dynamics between predators and prey being influenced by various factors. The introduction of spatial diffusion terms into the predator-prey model, as discussed in [22–27], enables a more precise description of the spatial distribution and dynamic changes of biological populations. This approach reveals intricate patterns of population size fluctuations, alterations in distribution patterns, and adjustments in competitive relationships, enhancing our understanding of ecosystem structure and function. Furthermore, spatial dispersal can give rise to Turing's patch diagrams [28–31], which play a crucial role in elucidating biodiversity maintenance, species distribution patterns, spatial heterogeneity, and ecosystem response and adaptation. The studies on spatial dispersal within predator-prey models have yielded significant outcomes in wildlife conservation, agriculture, fisheries management, ecology education, scientific research, and the popularization of science.

Since Alan Turing's [32] groundbreaking paper, the phenomenon of self-diffusion triggering self-organized patterning in reaction-diffusion systems has been extensively researched [33–35]. In the predator-prey model, self-diffusion vividly captures the migratory behaviors of individuals within

a population as they search for food or avoid overcrowding, significantly influencing the spatial arrangement and intrinsic mechanisms of population dynamics. On the other hand, the introduction of cross-diffusion portrays the complex dynamic interplay between predators and prey in a more detailed manner. The effects of cross-diffusion on various predator-prey models have been analyzed by researchers in references [36–42]. By simulating the predator's pursuit of prey and their mutual influence on spatial distribution and abundance, the cross-diffusion model provides a more realistic depiction of ecosystems. This model delves into the underlying mechanisms of predator-prey interactions and explores their impact on ecosystem stability, offering a comprehensive understanding of ecosystem complexity and diversity. Moreover, it enhances the accuracy and predictive capability of the model, providing valuable theoretical insights for the development of ecological conservation and management strategies.

In reference [43], a class of predator-prey models incorporating herd behavior and cross-diffusion was examined. Through calculations and analysis of the paradigm on the central manifold linked to the Turing-Hopf bifurcation, it was discovered that, under specific conditions, there is a diverse range of spatio-temporal dynamics near the Turing-Hopf bifurcation point.

Based on the available research data, it is evident that there are fewer studies on discrete predator-prey models, particularly those that incorporate herd behavior and diffusion. Therefore, our primary goal of this paper is to enhance models by introducing a cellular automaton (CML) model approach and diffusion factors. The predator-prey model that is discrete in both time and space can more accurately describe the spatial distribution of biological populations and the dynamics of quantitative changes. This model effectively addresses complex factors such as environmental resources, prey relationships, and competitive interactions, enabling greater flexibility in analysis. As a result, it enhances predictability and provides valuable insights for formulating ecological conservation strategies and managing biological resources. This innovative approach is designed to provide a more precise representation of real-world biological scenarios.

Here, we delve into the analysis of a CML model approach with the integration of diffusion factors to enhance predator-prey models. The discussion is structured into various sections: In Section 2, we examine the proposed model, while in Section 3, we analyze system behavior without diffusion, covering stability analysis, Neimark-Sacker bifurcation, and Flip bifurcation with normal forms provided. In Section 4, we explore Turing bifurcations under spatial inhomogeneities, and in Section 5, we present numerical simulations on asymptotic stabilization, Flip bifurcation, Neimark-Sacker bifurcation diagrams, and various Turing instabilities. These include pure Turing instability, Neimark-Sacker-Turing instability, Flip-Turing instability, spatially homogeneous stable state, spatially homogeneous periodic oscillation state, and spatially homogeneous period-doubling oscillatory state. Finally, we summarize our key findings in Section 6.

2. Model analysis

In [21], mathematical models are introduced and explored to examine the interplay between predators influenced by fear and the effects of group behavior.

$$\begin{cases} \frac{du}{dt} = ru(1-u)\left(\frac{1}{1+kv}\right) - \sqrt{u}v, \\ \frac{dv}{dt} = -\alpha v + \beta\sqrt{u}v. \end{cases} \tag{2.1}$$

Considering cross-diffusion in two dimensions, we obtain the following model:

$$\begin{cases} \frac{du}{dt} = ru(1-u)\left(\frac{1}{1+kv}\right) - \sqrt{u}v + d_{11}\left(\frac{\partial^2 u}{\partial x^2} + \frac{\partial^2 u}{\partial y^2}\right) + d_{12}\left(\frac{\partial^2 v}{\partial x^2} + \frac{\partial^2 v}{\partial y^2}\right), \\ \frac{dv}{dt} = -\alpha v + \beta\sqrt{u}v + d_{21}\left(\frac{\partial^2 u}{\partial x^2} + \frac{\partial^2 u}{\partial y^2}\right) + d_{22}\left(\frac{\partial^2 v}{\partial x^2} + \frac{\partial^2 v}{\partial y^2}\right). \end{cases} \tag{2.2}$$

The establishment of a coupled mapping lattice involves defining the $(m+2)\times(m+2)$, $m \in \mathbb{N}^+$ grid in a two-dimensional matrix region and discretizing time using the forward Euler method. The quantities of predators and prey on the (i, j) grid at time t are denoted by $u_n(i, j)$ and $v_n(i, j)$, respectively. This lattice functions to illustrate the population distribution of predators and prey across the grid. By incorporating spatial diffusion, the model (2.3) enables dynamic variations in biomass over time, reflecting the spatial dynamics of the predator-prey system.

$$\begin{cases} u_{n+1}(i, j) = f(u_n(i, j), v_n(i, j)) + \frac{d_{11}\tau}{h^2}\nabla^2 u_n(i, j) + \frac{d_{12}\tau}{h^2}\nabla^2 v_n(i, j), \\ v_{n+1}(i, j) = g(u_n(i, j), v_n(i, j)) + \frac{d_{21}\tau}{h^2}\nabla^2 u_n(i, j) + \frac{d_{22}\tau}{h^2}\nabla^2 v_n(i, j), \end{cases} \tag{2.3}$$

where

$$\begin{cases} f(u_n(i, j), v_n(i, j)) = u_n(i, j) + \tau r u_n(i, j)(1 - u_n(i, j))\left(\frac{1}{1+kv_n(i,j)}\right) - \tau\sqrt{u_n(i, j)}v_n(i, j), \\ g(u_n(i, j), v_n(i, j)) = v_n(i, j) - \tau\alpha v_n(i, j) + \tau\beta\sqrt{u_n(i, j)}v_n(i, j). \end{cases} \tag{2.4}$$

The variables i and j range from 0 to $m+1$, where i and j are integers. Here, τ denotes the time step, and h represents the spatial step. The cross-diffusion coefficients are denoted by d_{11}, d_{12}, d_{21}, and d_{22}, all of which are positive.

The discrete Laplacian can be defined in the following manner:

$$\begin{cases} \nabla^2 u_n(i, j) = u_n(i+1, j) + u_n(i-1, j) + u_n(i, j+1) + u_n(i, j-1) - 4u_n(i, j), \\ \nabla^2 v_n(i, j) = v_n(i+1, j) + v_n(i-1, j) + v_n(i, j+1) + v_n(i, j-1) - 4v_n(i, j). \end{cases} \tag{2.5}$$

The diffusion and response processes in the predator-prey model are inextricably linked, yet they can be interpreted to indicate a certain degree of "diffusion to find or avoid each other, followed by interaction within a given area". Accordingly, the model can be enhanced as follows:

First, diffusion occurs:

$$\begin{cases} \widetilde{u}_n(i, j) = u_n(i, j) + \frac{d_{11}\tau}{h^2}\nabla^2 u_n(i, j) + \frac{d_{12}\tau}{h^2}\nabla^2 v_n(i, j), \\ \widetilde{v}_n(i, j) = v_n(i, j) + \frac{d_{21}\tau}{h^2}\nabla^2 u_n(i, j) + \frac{d_{22}\tau}{h^2}\nabla^2 v_n(i, j). \end{cases} \tag{2.6}$$

Second, reaction occurs:

$$\begin{aligned} u_{n+1}(i, j) &= \widetilde{u}_n(i, j) + \tau r\widetilde{u}_n(i, j)(1 - \widetilde{u}_n(i, j))\left(\frac{1}{1+k\widetilde{v}_n(i,j)}\right) - \tau\sqrt{\widetilde{u}_n(i, j)}\widetilde{v}_n(i, j), \\ v_{n+1}(i, j) &= \widetilde{v}_n(i, j) - \tau\alpha\widetilde{v}_n(i, j) + \tau\beta\sqrt{\widetilde{u}_n(i, j)}\widetilde{v}_n(i, j), \end{aligned} \tag{2.7}$$

and satisfy the periodic boundary conditions

$$u_n(i, 0) = u_n(i, m),\ u_n(i, 1) = u_n(i, m+1),\ u_n(0, j) = u_n(m, j),\ u_n(1, j) = u_n(m+1, j),$$

$$v_n(i, 0) = v_n(i, m),\ v_n(i, 1) = v_n(i, m+1),\ v_n(0, j) = v_n(m, j),\ v_n(1, j) = v_n(m+1, j).$$

Remark 2.1. *In natural ecosystems, predators and prey occupy distinct habitats and have defined activity ranges. They engage in continuous movement and dispersion to seek out food, mates, or evade natural threats, a phase known as the "spreading" stage. When predators and prey encounter each other spatially, and the predator is poised to capture the prey, predatory behavior ensues promptly, marking the "reaction" stage. Consequently, the interaction between predators and prey adheres to a "diffusion followed by reaction" framework in a generalized sense. This conceptualization leads to the formulation of a model that captures the dynamic interplay between predators and prey.*

3. Analysis of kinetic properties without diffusion conditions

Without considering diffusion, the system can be described as follows:

$$\begin{cases} u_{n+1}(i,j) = u_n(i,j) + \tau r u_n(i,j)(1-u_n(i,j))\left(\frac{1}{1+kv_n(i,j)}\right) - \tau\sqrt{u_n(i,j)}v_n(i,j), \\ v_{n+1}(i,j) = v_n(i,j) - \tau\alpha v_n(i,j) + \tau\beta\sqrt{u_n(i,j)}v_n(i,j). \end{cases} \tag{3.1}$$

Since the concentration remains uniform across all locations on the plane when diffusion is not considered, the model can be simplified as follows:

$$\begin{cases} u_{n+1} = u_n + \tau r u_n(1-u_n)\left(\frac{1}{1+kv_n}\right) - \tau\sqrt{u_n}v_n, \\ v_{n+1} = v_n - \tau\alpha v_n + \tau\beta\sqrt{u_n}v_n. \end{cases} \tag{3.2}$$

3.1. Stability analysis of equilibrium points

By calculation, it can be determined that the model has trivial equilibrium points $E_0(0,0)$ and boundary equilibrium points $E_1(1,0)$.

(H) $\beta^3 + 4kr\alpha\beta^2 - 4kr\alpha^3 > 0$.

If condition (H) holds, then there exists a positive equilibrium point $E^*(u^*, v^*)$ of the system (3.2) at this point, where $u^* = \frac{\alpha^2}{\beta^2}$, $v^* = -\frac{1}{2k} + \frac{1}{2k}\sqrt{1 + 4k\frac{r\alpha}{\beta^3}(\beta^2 - \alpha^2)}$.

The Jacobi matrix for model (3.2) is

$$J = \begin{pmatrix} 1 + \tau\left(\frac{r-2ru}{1+kv} - \frac{v}{2\sqrt{u}}\right) & -\frac{\tau rku(1-u)}{(1+kv)^2} - \tau\sqrt{u} \\ \frac{\tau\beta v}{2\sqrt{u}} & 1 + \tau\left(\beta\sqrt{u} - \alpha\right) \end{pmatrix}. \tag{3.3}$$

Substituting the trivial equilibrium point $E_0(0,0)$ into the Jacobi matrix yields the corresponding characteristic equation, which in turn provides the eigenvalues $\lambda_{01} = 1 + \tau r$ and $\lambda_{02} = 1 - \tau\alpha$, respectively.

Theorem 3.1. *For trivial equilibrium point $E_0(0,0)$:*

(i) $E_0(0,0)$ is a source if $0 < \alpha < \frac{2}{\tau}$.

(ii) $E_0(0,0)$ is a saddle point if $\alpha > \frac{2}{\tau}$.

Similarly, the eigenvalues $\lambda_{11} = 1 - \tau r$, $\lambda_{12} = 1 + \tau(\beta - \alpha)$ can be obtained by substituting the boundary equilibrium point $E_1(1,0)$.

Theorem 3.2. *For boundary equilibrium point $E_1(1,0)$:*

(i) $E_1(1,0)$ is a sink, if $\beta < \alpha, 0 < r < \frac{2}{\tau}, 0 < \tau < \frac{2}{\alpha-\beta}$.

(ii) $E_1(1,0)$ is a source, if $\alpha < \beta, r > \frac{2}{\tau}$, or $\alpha > \beta + \frac{2}{\tau}, r > \frac{2}{\tau}$.

(iii) $E_1(1,0)$ is a saddle point, if $\alpha < \beta, 0 < r < \frac{2}{\tau}$, or $\alpha > \beta + \frac{2}{\tau}, 0 < r < \frac{2}{\tau}$.

For the positive equilibrium point $E^*(u^*, v^*)$, substituting it into the Jacobi matrix yields the corresponding characteristic equation as follows:

$$\lambda^2 - tr(\tau)\lambda + \det(\tau) = 0, \tag{3.4}$$

where $tr(\tau) = 2 + \tau\left(\frac{r-2ru^*}{1+kv^*} - \frac{v^*}{2\sqrt{u^*}}\right)$, $\det(\tau) = 1 + \frac{1}{2}\left(\beta\tau^2 v^* - \frac{\tau v^*}{\sqrt{u^*}} - \frac{kr\beta\tau^2(-1+u^*)\sqrt{u^*}v^*}{(1+kv^*)^2} + \frac{2\tau(r-2ru^*)}{1+kv^*}\right)$.

According to the Routh-Hurwitz criterion, the sufficient condition for local asymptotic stabilization at the positive equilibrium point is that the modulus of all eigenvalues at the equilibrium point is less than 1, i.e.,

$$\begin{cases} 1 - tr(\tau) + \det(\tau) > 0, \\ 1 + tr(\tau) + \det(\tau) > 0, \\ 1 - \det(\tau) > 0. \end{cases} \tag{3.5}$$

Theorem 3.3. *If Eq (3.5) holds, then the system is locally asymptotically stable at the positive equilibrium point.*

Remark 3.1. *A comprehensive examination of progressive stabilization in the predator-prey model is essential for advancing our understanding of the dynamic equilibrium mechanism between predators and prey within an ecosystem. This analysis not only demonstrates the capacity of ecosystems to restore equilibrium in the face of internal and external disturbances, but also provides indispensable theoretical support and a scientific foundation for the implementation of ecological conservation practices.*

3.2. Neimark-Sacker bifurcation analysis

Given that we are working with a predator-prey model, we analyze the positive equilibrium point $E^*(u^*, v^*)$ in all subsequent discussions to ensure its biological significance.

A Neimark-Sacker bifurcation occurs when characteristic equation (3.4) has a pair of complex conjugate roots of modulus 1. By treating the time step as a parameter, it is possible to determine the two eigenvalues of characteristic equation (3.4) as follows:

$$\lambda_{1,2}(\tau) = \frac{tr(\tau) \pm \sqrt{tr(\tau)^2 - 4\det(\tau)}}{2}. \tag{3.6}$$

The time step at which Neimark-Sacker bifurcations occur is designated as $\tau = \tau_1^*$. Considering the conditions for Neimark-Sacker bifurcations, we can ascertain the following:

$$\begin{cases} \det\left(\tau_1^*\right) = 1, \\ \left|tr\left(\tau_1^*\right)\right| < 2. \end{cases} \tag{3.7}$$

By calculation, we have

$$\begin{cases} \tau_1^* = \frac{(1+kv^*)\left(-2r\sqrt{u^*}+4r(u^*)^{3/2}+v^*+k(v^*)^2\right)}{\beta\sqrt{u^*}v^*\left(kr\sqrt{u^*}-kr(u^*)^{3/2}+(1+kv^*)^2\right)}, \\ \left|2 + \tau_1^*\left(\frac{r-2ru^*}{1+kv^*} - \frac{v^*}{2\sqrt{u^*}}\right)\right| < 2. \end{cases} \tag{3.8}$$

Furthermore, the following conditions must be satisfied:

$$(\lambda(\tau_1^*))^k \neq 1, 2, 3, 4. \tag{3.9}$$

For condition (3.9), it is equivalent that

$$tr\left(\tau_1^*\right) \neq -2, 0, 1, 2. \tag{3.10}$$

Since $\left|tr\left(\tau_1^*\right)\right| < 2$, so the condition changes to $tr\left(\tau_1^*\right) \neq 0, 1$, i.e.,

$$\frac{\left(-2r\sqrt{u^*} + 4r(u^*)^{3/2} + v^* + k(v^*)^2\right)^2}{2\beta u^* v^*\left(kr\sqrt{u^*} - kr(u^*)^{3/2} + (1+kv^*)^2\right)} \neq 1, 2. \tag{3.11}$$

It is important to emphasize that, in addition to the previously mentioned conditions, a Neimark-Sacker bifurcation can only occur if crosscut condition (3.12) is satisfied, i.e.,

$$d = \frac{\partial\left|\lambda_{1,2}(\tau)\right|^2}{\partial\tau}\Big|_{\tau=\tau_1^*} = \frac{\partial \det(\tau)}{\partial\tau}\Big|_{\tau=\tau_1^*} = \frac{-2r\sqrt{u^*} + 4r(u^*)^{3/2} + v^* + k(v^*)^2}{2\sqrt{u^*}(1+kv^*)} \neq 0. \tag{3.12}$$

The normal form of the Neimark-Sacker bifurcation is examined in the following section.

The initial step involves translating the system (3.2) from the positive equilibrium to the origin using the transformations: $u_{1,n} = u_n - u^*$ and $v_{1,n} = v_n - v^*$,

$$\begin{cases} u_{1,n+1} = u_{1,n} + \tau r(u_{1,n}+u^*)(1-(u_{1,n}+u^*))\left(\frac{1}{1+k(v_{1,n}+v^*)}\right) - \tau\sqrt{(u_{1,n}+u^*)}(v_{1,n}+v^*), \\ v_{1,n+1} = v_{1,n} - \tau\alpha(v_{1,n}+v^*) + \tau\beta\sqrt{(u_{1,n}+u^*)}(v_{1,n}+v^*). \end{cases} \tag{3.13}$$

By performing a Taylor expansion of the system at the origin $(u_{1,n}, v_{1,n}) = (0,0)$, we obtain the following result:

$$\begin{cases} u_{1,n+1} = a_{10}u_{1,n} + a_{01}v_{1,n} + f_{11}(u_{1,n}, v_{1,n}) + O\left(\left(\left|u_{1,n}\right| + \left|v_{1,n}\right|\right)^4\right), \\ v_{1,n+1} = b_{10}u_{2,n} + b_{01}v_{1,n} + g_{21}(u_{1,n}, v_{1,n}) + O\left(\left(\left|v_{1,n}\right| + \left|v_{1,n}\right|\right)^4\right), \end{cases} \tag{3.14}$$

where

$$f_{11}(u_{1,n}, v_{1,n}) = a_{20}(u_{1,n})^2 + a_{11}u_{1,n}v_{1,n} + a_{02}(v_{1,n})^2 + a_{30}(u_{1,n})^3 + a_{21}(u_{2,n})^2v_{1,n} + a_{12}u_{1,n}(v_{1,n})^2 + a_{03}(v_{1,n})^3,$$

$$g_{11}(u_{1,n}, v_{1,n}) = b_{20}(u_{1,n})^2 + b_{11}u_{1,n}v_{1,n} + b_{02}(v_{1,n})^2 + b_{30}(u_{1,n})^3 + b_{21}(u_{2,n})^2v_{1,n} + b_{12}u_{1,n}(v_{1,n})^2 + b_{03}(v_{1,n})^3,$$

$$a_{10} = 1 - \frac{\tau v^*}{2\sqrt{u^*}} + \frac{r\tau(1-2u^*)}{1+kv^*},\ a_{01} = -\tau\sqrt{u^*} + \frac{kr\tau(-1+u^*)u^*}{(1+kv^*)^2},\ a_{20} = \frac{\tau v^*}{8(u^*)^{3/2}} - \frac{r\tau}{1+kv^*},$$

$$a_{11} = -\frac{\tau}{2\sqrt{u^*}} + \frac{kr\tau(-1+2u^*)}{(1+kv^*)^2},\ a_{02} = -\frac{k^2r\tau(-1+u^*)u^*}{(1+kv^*)^3},\ a_{30} = -\frac{\tau v^*}{16(u^*)^{5/2}},$$

$$a_{21} = \frac{\tau}{8(u^*)^{3/2}} + \frac{kr\tau}{(1+kv^*)^2},\ a_{12} = \frac{k^2r\tau(1-2u^*)}{(1+kv^*)^3},\ a_{03} = \frac{k^3r\tau(-1+u^*)u^*}{(1+kv^*)^4},$$

$$b_{10} = \frac{\beta\tau v^*}{2\sqrt{u^*}},\ b_{10} = \frac{\beta\tau v^*}{2\sqrt{u^*}},\ b_{01} = 1 - \alpha\tau + \beta\tau\sqrt{u^*},\ b_{20} = -\frac{\beta\tau v^*}{8(u^*)^{3/2}},$$

$$b_{11} = \frac{\beta\tau}{2\sqrt{u^*}},\ b_{30} = \frac{\beta\tau v^*}{16(u^*)^{5/2}},\ b_{21} = -\frac{\beta\tau}{8(u^*)^{3/2}},\ b_{02} = b_{12} = b_{03} = 0.$$

Ignoring the quadratic term $O\left(\left(\left|u_{1,n}\right| + \left|v_{1,n}\right|\right)^4\right)$, the system can be reformulated as follows:

$$\begin{pmatrix} u_{1,n+1} \\ v_{1,n+1} \end{pmatrix} = \begin{pmatrix} 1 - \frac{\tau v^*}{2\sqrt{u^*}} + \frac{r\tau(1-2u^*)}{1+kv^*} & -\tau\sqrt{u^*} + \frac{kr\tau(-1+u^*)u^*}{(1+kv^*)^2} \\ \frac{\beta\tau v^*}{2\sqrt{u^*}} & 1 - \alpha\tau + \beta\tau\sqrt{u^*} \end{pmatrix} \begin{pmatrix} u_{1,n} \\ v_{1,n} \end{pmatrix} + \begin{pmatrix} f_{11}\left(u_{1,n}, v_{1,n}\right) \\ g_{11}\left(u_{1,n}, v_{1,n}\right) \end{pmatrix}. \tag{3.15}$$

In the event that the Neimark-Sacker bifurcation condition is satisfied, the eigenvalues can be expressed as complex numbers.

$$\lambda_{1,2}\left(\tau_1^*\right) = \frac{tr\left(\tau_1^*\right) \pm i\sqrt{4\det\left(\tau_1^*\right) - tr\left(\tau_1^*\right)^2}}{2} = \omega_1 \pm i\omega_2. \tag{3.16}$$

The following transformation is applied:

$$\begin{pmatrix} u_{1,n} \\ v_{1,n} \end{pmatrix} = \begin{pmatrix} a_{01} & 0 \\ \omega_1 - a_{10} & -\omega_2 \end{pmatrix} \begin{pmatrix} U_{1,n} \\ V_{1,n} \end{pmatrix}. \tag{3.17}$$

The model (3.15) becomes

$$\begin{pmatrix} U_{1,n+1} \\ V_{1,n+1} \end{pmatrix} = \begin{pmatrix} \omega_1 & -\omega_2 \\ \omega_2 & \omega_1 \end{pmatrix} \begin{pmatrix} U_{1,n} \\ V_{1,n} \end{pmatrix} + \begin{pmatrix} f_{12}\left(U_{1,n}, V_{1,n}\right) \\ g_{12}\left(U_{1,n}, V_{1,n}\right) \end{pmatrix}, \tag{3.18}$$

where

$$\begin{pmatrix} f_{12}\left(U_{1,n}, V_{1,n}\right) \\ g_{12}\left(U_{1,n}, V_{1,n}\right) \end{pmatrix} = \begin{pmatrix} a_{01} & 0 \\ \omega_1 - a_{10} & -\omega_2 \end{pmatrix}^{-1} \begin{pmatrix} f_{11}\left(a_{01}U_{1,n}, (\omega_1 - a_{10})U_{1,n} - \omega_2 V_{1,n}\right) \\ g_{11}\left(a_{01}U_{1,n}, (\omega_1 - a_{10})U_{1,n} - \omega_2 V_{1,n}\right) \end{pmatrix}. \tag{3.19}$$

Based on reference [43], system (3.2) undergoes a Neimark-Sacker bifurcation at $E^*\left(u^*, v^*\right)$ and needs to meet the following criteria:

$$\rho = -\mathrm{Re}\left(\frac{(1-2\lambda_1)\lambda_2^2}{1-\lambda_1}\xi_{11}\xi_{20}\right) - \frac{1}{2}|\xi_{11}|^2 - |\xi_{02}|^2 + \mathrm{Re}\left(\lambda_2\xi_{21}\right) \neq 0, \tag{3.20}$$

where the corresponding coefficients are provided in Appendix A.

Theorem 3.4. *If conditions (3.8), (3.11), (3.12), and (3.20) are satisfied, the system described by Eq (3.2) will experience a Neimark-Sacker bifurcation at the time $\tau = \tau_1^*$. Furthermore, if ρ is less than zero, the Neimark-Sacker bifurcation is classified as supercritical, resulting in the generation of a stable periodic oscillation.*

Remark 3.2. *Through examination, we can gain valuable insights into how the dynamic equilibrium between predator and prey populations is influenced by the system's parameters. In cases where the Neimark-Sacker bifurcation is supercritical, the system exhibits stable periodic oscillations, indicating a consistent pattern in the interactions between predator and prey populations. Altering specific parameters in the model can lead to the destabilization of initially stable periodic orbits due to the Neimark-Sacker bifurcation, giving rise to complex quasi-periodic or chaotic behaviors. This process not only reveals the intricacies of the interaction mechanisms between predators and prey but also showcases the dynamic evolution that ecosystems may experience when facing internal and external disturbances.*

3.3. Flip bifurcation analysis

In the context of a Flip bifurcation, characteristic equation (3.4) exhibits one characteristic value of -1, while the other has a modulus less than one. By treating the time step as a parameter, the two eigenvalues of characteristic equation (3.4) can be determined as follows: $\lambda_1(\tau) = -1$, $\lambda_2(\tau) = tr(\tau) + 1$.

The time step at which Flip bifurcations occur is designated as $\tau = \tau_2^*$. In light of the conditions governing Flip bifurcations, the following can be ascertained:

$$\begin{cases} 1 + tr\left(\tau_2^*\right) + \det\left(\tau_2^*\right) = 0, \\ \left|tr\left(\tau_2^*\right) + 1\right| < 1. \end{cases} \tag{3.21}$$

By calculation, we have

$$\begin{cases} \tau_2^* = \frac{(1+kv^*)^2}{\beta v^* \kappa}\left(\frac{v^*}{\sqrt{u^*}} - \frac{2r}{1+kv^*} + \frac{4ru^*}{1+kv^*} \pm \sqrt{\varsigma}\right), \\ 2 < \tau\left(\frac{v^*}{2\sqrt{u^*}} - \frac{r-2ru^*}{1+kv^*}\right) < 4, \end{cases} \tag{3.22}$$

where $\kappa = kr\sqrt{u^*} - kr(u^*)^{3/2} + (1+kv^*)^2$, $\varsigma = \frac{\left(-2r\sqrt{u^*}+4r(u^*)^{3/2}+v^*+k(v^*)^2\right)^2 - 8\beta u^* v^* \kappa}{u^*(1+kv^*)^2}$.

The discussion provided focuses solely on $\tau_2^* = \frac{(1+kv^*)^2}{\beta v^* \kappa}\left(\frac{v^*}{\sqrt{u^*}} - \frac{2r}{1+kv^*} + \frac{4ru^*}{1+kv^*} + \sqrt{\varsigma}\right)$. The alternative case, $\tau_2^* = \frac{(1+kv^*)^2}{\beta v^* \kappa}\left(\frac{v^*}{\sqrt{u^*}} - \frac{2r}{1+kv^*} + \frac{4ru^*}{1+kv^*} - \sqrt{\varsigma}\right)$, can be obtained through a similar approach.

The normal form of the Flip bifurcation will be examined in the following section.

First, we move the system from the positive equilibrium to the origin using the transformations $u_{2,n} = u_n - u^*$, $v_{2,n} = v_n - v^*$, $\widetilde{\tau} = \tau - \tau_2^*$, which enables us to obtain the following result:

$$\begin{cases} u_{2,n+1} = u_{2,n} + \left(\widetilde{\tau} + \tau_2^*\right)\left(r\left(u_{2,n}+u^*\right)\left(1 - \left(u_{2,n}+u^*\right)\right)\left(\frac{1}{1+k\left(v_{2,n}+v^*\right)}\right) - \sqrt{\left(u_{2,n}+u^*\right)}\left(v_{2,n}+v^*\right)\right), \\ v_{2,n+1} = v_{2,n} - \left(\widetilde{\tau} + \tau_2^*\right)\alpha\left(v_{2,n}+v^*\right) + \tau\beta\sqrt{\left(u_{2,n}+u^*\right)}\left(v_{2,n}+v^*\right). \end{cases} \tag{3.23}$$

Performing a Taylor expansion of the system at the origin $\left(u_{2,n}, v_{2,n}, \tau_2^*\right) = (0,0,0)$, we obtain the following result:

$$\begin{cases} u_{2,n+1} = a_{100}u_{2,n} + a_{010}v_{2,n} + a_{001}\widetilde{\tau} + f_{21}\left(u_{2,n}, v_{2,n}, \widetilde{\tau}\right) + O\left(\left(\left|u_{2,n}\right| + \left|v_{2,n}\right| + \left|\widetilde{\tau}\right|\right)^4\right), \\ v_{2,n+1} = b_{100}u_{2,n} + b_{010}v_{2,n} + b_{001}\widetilde{\tau} + g_{21}\left(u_{2,n}, v_{2,n}, \widetilde{\tau}\right) + O\left(\left(\left|u_{2,n}\right| + \left|v_{2,n}\right| + \left|\widetilde{\tau}\right|\right)^4\right), \end{cases} \tag{3.24}$$

where the corresponding coefficients are given in Appendix B.

Ignoring the quadratic term $O\left(\left(\left|u_{2,n}\right| + \left|v_{2,n}\right| + \left|\widetilde{\tau}\right|\right)^4\right)$, the system can be rewritten as

$$\begin{pmatrix} u_{2,n+1} \\ v_{2,n+1} \end{pmatrix} = \begin{pmatrix} 1 - \frac{\tau_2^* v^*}{2\sqrt{u^*}} + \frac{r\tau_2^*(1-2u^*)}{1+kv^*} & -\tau_2^*\sqrt{u^*} + \frac{kr\tau_2^*(-1+u^*)u^*}{(1+kv^*)^2} \\ \frac{\beta\tau_2^* v^*}{2\sqrt{u^*}} & 1 - \alpha\tau_2^* + \beta\tau_2^*\sqrt{u^*} \end{pmatrix}\begin{pmatrix} u_{2,n} \\ v_{2,n} \end{pmatrix} + \begin{pmatrix} f_{21}\left(u_{2,n}, v_{2,n}, \widetilde{\tau}\right) \\ g_{21}\left(u_{2,n}, v_{2,n}, \widetilde{\tau}\right) \end{pmatrix}. \tag{3.25}$$

The following transformation is applied:

$$\begin{pmatrix} u_{2,n} \\ v_{2,n} \end{pmatrix} = \begin{pmatrix} a_{010} & a_{010} \\ -1 - a_{100} & \lambda_2 - a_{100} \end{pmatrix}\begin{pmatrix} U_{2,n} \\ V_{2,n} \end{pmatrix} = A\begin{pmatrix} U_{2,n} \\ V_{2,n} \end{pmatrix}. \tag{3.26}$$

Model (3.25) becomes

$$\begin{pmatrix} U_{2,n+1} \\ V_{2,n+1} \end{pmatrix} = \begin{pmatrix} -1 & 0 \\ 0 & \lambda_2 \end{pmatrix} \begin{pmatrix} U_{2,n} \\ V_{2,n} \end{pmatrix} + \begin{pmatrix} f_{22}\left(U_{2,n}, V_{2,n}, \widetilde{\tau}\right) \\ g_{22}\left(U_{2,n}, V_{2,n}, \widetilde{\tau}\right) \end{pmatrix}, \tag{3.27}$$

where

$$\begin{pmatrix} f_{22}\left(U_{2,n}, V_{2,n}, \widetilde{\tau}\right) \\ g_{22}\left(U_{2,n}, V_{2,n}, \widetilde{\tau}\right) \end{pmatrix} = A^{-1} \begin{pmatrix} f_{21}\left(a_{010}U_{2,n} + a_{010}V_{2,n}, (-1-a_{100})U_{2,n} + (\lambda_2 - a_{100})V_{2,n}, \widetilde{\tau}\right) \\ g_{21}\left(a_{010}U_{2,n} + a_{010}V_{2,n}, (-1-a_{100})U_{2,n} + (\lambda_2 - a_{100})V_{2,n}, \widetilde{\tau}\right) \end{pmatrix}. \tag{3.28}$$

Therefore, we can obtain

$$\begin{pmatrix} U_{2,n+1} \\ V_{2,n+1} \\ \widetilde{\tau} \end{pmatrix} = \begin{pmatrix} -1 & 0 & 0 \\ 0 & \lambda_2 & 0 \\ 0 & 0 & 1 \end{pmatrix} \begin{pmatrix} U_{2,n} \\ V_{2,n} \\ \widetilde{\tau} \end{pmatrix} + \begin{pmatrix} f_{22}\left(U_{2,n}, V_{2,n}, \widetilde{\tau}\right) \\ g_{22}\left(U_{2,n}, V_{2,n}, \widetilde{\tau}\right) \\ 0 \end{pmatrix}. \tag{3.29}$$

The center prevalence at the origin can be expressed as follows:

$$W^C(0,0,0) = \left\{ \left(U_{2,n}, V_{2,n}, \widetilde{\tau}\right) \in \mathbb{R}^3 | V_{2,n} = z^*\left(U_{2,n}, \widetilde{\tau}\right), z^*(0,0) = 0, Dz^*(0,0) = 0 \right\}, \tag{3.30}$$

where

$$z^*\left(U_{2,n}, \widetilde{\tau}\right) = e_1 (U_{2,n})^2 + e_2 U_{2,n}\widetilde{\tau} + e_3 (\widetilde{\tau})^2 + O\left(\left(\left|U_{2,n}\right| + |\widetilde{\tau}|\right)^3\right). \tag{3.31}$$

Therefore, we can obtain

$$\begin{aligned} &e_1(-U_{2,n} + f_{12}\left(U_{2,n}, z^*\left(U_{2,n}, \widetilde{\tau}\right), \widetilde{\tau}\right))^2 + e_2\left(-U_{2,n} + f_{12}\left(U_{2,n}, z^*\left(U_{2,n}, \widetilde{\tau}\right), \widetilde{\tau}\right)\right)\widetilde{\tau} + e_3(\widetilde{\tau})^2 - \lambda_2 e_1 (U_{2,n})^2 \\ &-\lambda_2\left(e_2 U_{2,n}\widetilde{\tau} + e_3(\widetilde{\tau})^2\right) - g_{12}\left(U_{2,n}, z^*\left(U_{2,n}, \widetilde{\tau}\right), \widetilde{\tau}\right) = O\left(\left(\left|U_{2,n}\right| + |\widetilde{\tau}|\right)^3\right). \end{aligned}$$

By comparing the quadratic coefficients, we can determine the coefficients as follows:

$$\begin{aligned} e_1 =& -\frac{1}{2a_{010}(-1+\lambda_2)(1+\lambda_2)}(a_{020}(1+a_{100})^3 + a_{010}\left(-2(1+a_{100})^2 a_{110} + (1+a_{100})^2 b_{020}\right. \\ &\left. + a_{010}(1+a_{100})(a_{200} - 2b_{110}) + {a_{010}}^2 b_{200}\right), \\ e_2 =& \frac{1}{a_{010}(1+\lambda_2)^2}\left(a_{011}(1+a_{100})^2 - a_{010}\left((1+a_{100})a_{101} - (1+a_{100})b_{011} + a_{010}b_{101}\right)\right), \\ e_3 =& -\frac{1}{2a_{010}(-1+\lambda_2)(1+\lambda_2)}\left(a_{002} + a_{002}a_{100} + a_{010}b_{002}\right). \end{aligned} \tag{3.32}$$

In accordance with the findings presented in (3.29), (3.31), and (3.32), we can conclude that

$$L\left(U_{2,n}, \widetilde{\tau}\right) = U_{n+1} = -U_{2,n} + f_{22}\left(U_{2,n}, z^*\left(U_{2,n}, \widetilde{\tau}\right), \widetilde{\tau}\right). \tag{3.33}$$

As indicated in [44], the occurrence of a Flip bifurcation requires that both the values of η_1 and η_2 are non-zero.

$$\begin{aligned} \eta_1 =& \left(\frac{\partial^2 L\left(U_{2,n}, \widetilde{\tau}\right)}{\partial U_{2,n}\partial\widetilde{\tau}} + \frac{1}{2}\frac{\partial L\left(U_{2,n}, \widetilde{\tau}\right)}{\partial\widetilde{\tau}}\frac{\partial^2 L\left(U_{2,n}, \widetilde{\tau}\right)}{\partial U_{2,n}^2}\right)\Big|_{\left(U_{2,n}, \widetilde{\tau}\right)=(0,0)} \neq 0, \\ \eta_2 =& \left(\frac{1}{6}\frac{\partial^3 L\left(U_{2,n}, \widetilde{\tau}\right)}{\partial U_{2,n}^3} + \left(\frac{1}{2}\frac{\partial^2 L\left(U_{2,n}, \widetilde{\tau}\right)}{\partial U_{2,n}^2}\right)^2\right)\Big|_{\left(U_{2,n}, \widetilde{\tau}\right)=(0,0)} \neq 0. \end{aligned} \tag{3.34}$$

Theorem 3.5. *If the conditions (3.22) are satisfied with $\eta_1 \neq 0$ and $\eta_2 \neq 0$, the system described by Eq (3.2) will experience a Flip bifurcation at the time $\tau = \tau_2^*$. Moreover, the stability of the Flip bifurcation is contingent on the sign of η_2: Stability occurs for $\eta_2 > 0$, while instability arises for $\eta_2 < 0$.*

Remark 3.3. *Flip bifurcation plays a crucial role in predator-prey models by revealing the nonlinear characteristics of ecosystem population dynamics and enhancing our understanding of the intricate interactions between predators and prey. As system parameters approach the Flip bifurcation point, population size fluctuations can become notably drastic, indicating dynamic shifts and potential crises within the ecosystem. By forecasting periodic changes in predator and prey populations, Flip bifurcation offers vital scientific support for ecological conservation and management.*

4. Turing instability analysis

Turing instability refers to the phenomenon where a system, which is stable in the absence of diffusion, becomes unstable in an inhomogeneous space due to the presence of diffusion. In the following section, we examine the circumstances under which instability arises in spatially inhomogeneous systems.

To obtain the conditions for Turing instability, we consider

$$\nabla^2 X^{i,j} + \lambda X^{i,j} = 0, \tag{4.1}$$

which satisfies the periodic boundary conditions: $X^{i,0} = X^{i,m}$, $X^{i,1} = X^{i,m+1}$, $X^{0,j} = X^{m,j}$, $X^{1,j} = X^{m+1,j}$.

In accordance with the stipulations set forth in [45], the variable $X^{i,j} = x^i y^j$ $(x \neq 0, y \neq 0)$, as introduced in (4.1), can be expressed as

$$\lambda = -\left(x + y + x^{-1} + y^{-1} - 4\right). \tag{4.2}$$

According to the periodic boundary conditions, we have $x^m = 1$, $y^m = 1$, which can be restated as

$$x_l = e^{\frac{2(l-1)\pi}{m} i},\ y_s = e^{\frac{2(s-1)\pi}{m} i}, \tag{4.3}$$

here, l and s are positive integers, with $1 \leq l, s \leq m$.

Upon substituting Eq (4.3) into Eq (4.2), the eigenvalue expression of Eq (4.1) is structured as follows:

$$\lambda_{l,s} = k_{l,s}^2 = 4\left(\sin^2\frac{(l-1)\pi}{m} + \sin^2\frac{(s-1)\pi}{m}\right) \triangleq 4\left(\sin^2\phi_l + \sin^2\phi_s\right). \tag{4.4}$$

In this context, the eigenfunction corresponding to the eigenvalue $\lambda_{l,s}$ is denoted as $X_{l,s}^{i,j}$, i.e.,

$$\nabla^2 X_{l,s}^{i,j} + \lambda_{l,s} X_{l,s}^{i,j} = 0. \tag{4.5}$$

The following part examines the stability of $E^*(u^*, v^*)$ in the presence of small-space heterogeneous perturbations.

Let $\widetilde{u}_n(i,j) = u_n(i,j) - u^*$, $\widetilde{v}_n(i,j) = v_n(i,j) - v^*$. Since $\nabla^2 u_n(i,j) = \nabla^2\widetilde{u}_n(i,j)$, $\nabla^2 v_n(i,j) = \nabla^2\widetilde{v}_n(i,j)$, we have

$$\begin{cases} \widetilde{u}_{n+1}(i,j) = a_{10}\left(\widetilde{u}_n(i,j) + \frac{\tau}{h^2}d_{11}\nabla^2\widetilde{u}_n(i,j) + \frac{\tau}{h^2}d_{12}\nabla^2\widetilde{v}_n(i,j)\right) + a_{01}\left(\widetilde{v}_n(i,j) + \frac{\tau}{h^2}d_{21}\nabla^2\widetilde{u}_n(i,j)\right. \\ \qquad\qquad \left. + \frac{\tau}{h^2}d_{22}\nabla^2\widetilde{v}_n(i,j)\right) + O\left(\left(|\widetilde{u}_n(i,j)| + |\widetilde{v}_n(i,j)|\right)^2\right), \\ \widetilde{v}_{n+1}(i,j) = b_{10}\left(\widetilde{u}_n(i,j) + \frac{\tau}{h^2}d_{11}\nabla^2\widetilde{u}_n(i,j) + \frac{\tau}{h^2}d_{12}\nabla^2\widetilde{v}_n(i,j)\right) + b_{01}\left(\widetilde{v}_n(i,j) + \frac{\tau}{h^2}d_{21}\nabla^2\widetilde{u}_n(i,j)\right. \\ \qquad\qquad \left. + \frac{\tau}{h^2}d_{22}\nabla^2\widetilde{v}_n(i,j)\right) + O\left(\left(|\widetilde{u}_n(i,j)| + |\widetilde{v}_n(i,j)|\right)^2\right). \end{cases} \tag{4.6}$$

In this case, a_{10}, a_{01}, b_{10}, and b_{01} are equivalent to the coefficients of the Neimark-Sacker bifurcation expansion in system (3.14). When the perturbation is small, the $O\left(\left(|\widetilde{u}_n(i,j)| + |\widetilde{v}_n(i,j)|\right)^2\right)$ term can be disregarded to simplify the linear system as follows:

$$\begin{cases} \widetilde{u}_{n+1}(i,j) = a_{10}\left(\widetilde{u}_n(i,j) + \frac{\tau}{h^2}d_{11}\nabla^2\widetilde{u}_n(i,j) + \frac{\tau}{h^2}d_{12}\nabla^2\widetilde{v}_n(i,j)\right) + a_{01}\left(\widetilde{v}_n(i,j) + \frac{\tau}{h^2}d_{21}\nabla^2\widetilde{u}_n(i,j)\right. \\ \qquad\qquad \left. + \frac{\tau}{h^2}d_{22}\nabla^2\widetilde{v}_n(i,j)\right), \\ \widetilde{v}_{n+1}(i,j) = b_{10}\left(\widetilde{u}_n(i,j) + \frac{\tau}{h^2}d_{11}\nabla^2\widetilde{u}_n(i,j) + \frac{\tau}{h^2}d_{12}\nabla^2\widetilde{v}_n(i,j)\right) + b_{01}\left(\widetilde{v}_n(i,j) + \frac{\tau}{h^2}d_{21}\nabla^2\widetilde{u}_n(i,j)\right. \\ \qquad\qquad \left. + \frac{\tau}{h^2}d_{22}\nabla^2\widetilde{v}_n(i,j)\right). \end{cases} \tag{4.7}$$

The system (4.7) is then multiplied by $X_{l,s}^{i,j}$ on both sides simultaneously.

$$\begin{cases} X_{l,s}^{i,j}\widetilde{u}_{n+1}(i,j) = X_{l,s}^{i,j}\left(a_{10}\widetilde{u}_n(i,j) + a_{01}\widetilde{v}_n(i,j)\right) + \frac{\tau}{h^2}X_{l,s}^{i,j}\left(a_{10}d_{11}\nabla^2\widetilde{u}_n(i,j) + a_{10}d_{12}\nabla^2\widetilde{v}_n(i,j)\right. \\ \qquad\qquad \left. + a_{01}d_{21}\nabla^2\widetilde{u}_n(i,j) + a_{01}d_{22}\nabla^2\widetilde{v}_n(i,j)\right), \\ X_{l,s}^{i,j}\widetilde{v}_{n+1}(i,j) = X_{l,s}^{i,j}\left(b_{10}\widetilde{u}_n(i,j) + a_{01}\widetilde{v}_n(i,j)\right) + \frac{\tau}{h^2}X_{l,s}^{i,j}\left(b_{10}d_{11}\nabla^2\widetilde{u}_n(i,j) + b_{10}d_{12}\nabla^2\widetilde{v}_n(i,j)\right. \\ \qquad\qquad \left. + b_{01}d_{21}\nabla^2\widetilde{u}_n(i,j) + b_{01}d_{22}\nabla^2\widetilde{v}_n(i,j)\right). \end{cases} \tag{4.8}$$

By adding up the values of i and j appearing in the above equation, we can obtain

$$\begin{cases} \sum_{i,j=1}^{m} X_{l,s}^{i,j}\widetilde{u}_{n+1}(i,j) = a_{10}\left(\sum_{i,j=1}^{m} X_{l,s}^{i,j}\widetilde{u}_n(i,j) + \frac{\tau}{h^2}d_{11}\sum_{i,j=1}^{m} X_{l,s}^{i,j}\nabla^2\widetilde{u}_n(i,j) + \frac{\tau}{h^2}d_{12}\sum_{i,j=1}^{m} X_{l,s}^{i,j}\nabla^2\widetilde{v}_n(i,j)\right) \\ \qquad\qquad + a_{01}\left(\sum_{i,j=1}^{m} X_{l,s}^{i,j}\widetilde{v}_n(i,j) + \frac{\tau}{h^2}d_{21}\sum_{i,j=1}^{m} X_{l,s}^{i,j}\nabla^2\widetilde{u}_n(i,j) + \frac{\tau}{h^2}d_{22}\sum_{i,j=1}^{m} X_{l,s}^{i,j}\nabla^2\widetilde{v}_n(i,j)\right), \\ \sum_{i,j=1}^{m} X_{l,s}^{i,j}\widetilde{v}_{n+1}(i,j) = b_{10}\left(\sum_{i,j=1}^{m} X_{l,s}^{i,j}\widetilde{u}_n(i,j) + \frac{\tau}{h^2}d_{11}\sum_{i,j=1}^{m} X_{l,s}^{i,j}\nabla^2\widetilde{u}_n(i,j) + \frac{\tau}{h^2}d_{12}\sum_{i,j=1}^{m} X_{l,s}^{i,j}\nabla^2\widetilde{v}_n(i,j)\right) \\ \qquad\qquad + b_{01}\left(\sum_{i,j=1}^{m} X_{l,s}^{i,j}\widetilde{v}_n(i,j) + \frac{\tau}{h^2}d_{21}\sum_{i,j=1}^{m} X_{l,s}^{i,j}\nabla^2\widetilde{u}_n(i,j) + \frac{\tau}{h^2}d_{22}\sum_{i,j=1}^{m} X_{l,s}^{i,j}\nabla^2\widetilde{v}_n(i,j)\right). \end{cases} \tag{4.9}$$

Based on reference [35], by introducing variables $\overline{u}_n = \sum_{i,j=1}^{m} X_{l,s}^{i,j} \widetilde{u}_n(i,j)$ and $\overline{v}_n = \sum_{i,j=1}^{m} X_{l,s}^{i,j} \widetilde{v}_n(i,j)$ and incorporating Eq (4.9), we can proceed to simplify the expression as follows:

$$\begin{cases} \overline{u}_{n+1} = \left(a_{10} - \frac{\tau}{h^2}\left(a_{10}d_{11} + a_{01}d_{21}\right)k_{l,s}^2\right)\overline{u}_n + \left(a_{01} - \frac{\tau}{h^2}\left(a_{10}d_{12} + a_{01}d_{22}\right)k_{l,s}^2\right)\overline{v}_n, \\ \overline{v}_{n+1} = \left(b_{10} - \frac{\tau}{h^2}\left(b_{10}d_{11} + b_{01}d_{21}\right)k_{l,s}^2\right)\overline{u}_n + \left(b_{01} - \frac{\tau}{h^2}\left(b_{10}d_{12} + b_{01}d_{22}\right)k_{l,s}^2\right)\overline{v}_n. \end{cases} \tag{4.10}$$

The stability of the solutions of systems (4.7) and (4.10) is interconnected. In the subsequent analysis, we derive the instability conditions of system (4.7) primarily through the examination of system (4.10).

The Jacobi matrix of system (4.10) is given by

$$\begin{pmatrix} a_{10} - \frac{\tau}{h^2}\left(a_{10}d_{11} + a_{01}d_{21}\right)k_{l,s}^2 & a_{01} - \frac{\tau}{h^2}\left(a_{10}d_{12} + a_{01}d_{22}\right)k_{l,s}^2 \\ b_{10} - \frac{\tau}{h^2}\left(b_{10}d_{11} + b_{01}d_{21}\right)k_{l,s}^2 & b_{01} - \frac{\tau}{h^2}\left(b_{10}d_{12} + b_{01}d_{22}\right)k_{l,s}^2 \end{pmatrix}. \tag{4.11}$$

Consequently, the characteristic equation can be derived.

$$\lambda^2 + M\left(k_{l,s}^2\right)\lambda + N\left(k_{l,s}^2\right) = 0, \tag{4.12}$$

where

$$M\left(k_{l,s}^2\right) = a_{10} + b_{01} - \frac{\tau}{h^2}k_{l,s}^2\left(a_{10}d_{11} + a_{01}d_{21} + b_{10}d_{12} + b_{01}d_{22}\right),$$

$$N\left(k_{l,s}^2\right) = \frac{1}{h^4}\left(a_{10}b_{01} - a_{01}b_{10}\right) * \left(h^4 - h^2\tau k_{l,s}^2\left(d_{11} + d_{22}\right) - \tau^2 k_{l,s}^4\left(d_{11}d_{22} - d_{12}d_{21}\right)\right).$$

At this juncture, the eigenvalues can be expressed as

$$\lambda_{1,2}\left(k_{l,s}^2\right) = \frac{M\left(k_{l,s}^2\right) \pm \sqrt{M^2\left(k_{l,s}^2\right) - 4N\left(k_{l,s}^2\right)}}{2}, \tag{4.13}$$

where $l, s \in \mathbb{Z}^+$, $1 \le s, l \le m$.

The critical value of the Turing bifurcation being $\left|\lambda_{12}\left(k_{l,s}^2\right)\right| = 1$ implies that if there are eigenvalues with a modulus greater than 1, i.e., $\left|\lambda_{12}\left(k_{l,s}^2\right)\right| > 1$, the system (4.10) will be in an unstable state.

We define $P(l,s) = \max\left\{\left|\lambda_1\left(k_{l,s}^2\right)\right|, \left|\lambda_2\left(k_{l,s}^2\right)\right|\right\}$, $P_m = \max_{l,s=1}^{m}\{P(l,s)\}$. Subsequently, we can derive the following theorem.

Theorem 4.1. *The following theorem characterizes the conditions under which systems (2.6) and (2.7) exhibit various types of instability:*

(i) Pure Turing instability occurs in systems (2.6) and (2.7) if either condition (3.5) holds and $P_{max} > 1$.

(ii) Neimark-Sacker-Turing instability arises in systems (2.6) and (2.7) when conditions (3.8), (3.11), (3.12), (3.20), and $P_{max} > 1$ *are satisfied.*

(iii) Flip-Turing instability is present in systems (2.6) and (2.7) if condition (3.22), $\eta_1 \neq 0$, $\eta_2 \neq 0$, *and* $P_{max} > 1$ *are met.*

Remark 4.1. *The significance of Turing instability analysis in biology mainly lies in revealing the complex spatial distribution patterns between predators and prey, such as speckled and striped patterns, which have a significant impact on the survival of species and the structure and function of ecosystems. In addition, the analysis helps to understand the cyclical fluctuations of species populations, reflecting the dynamic balance of ecosystems and providing a scientific basis for predicting population trends. Turing analysis also explores non-linear dynamic behavior in ecosystems, including chaos and bifurcation phenomena, demonstrating the high sensitivity of ecosystems to environmental changes, where small alterations can lead to significant ecological consequences. Such analyses have advanced ecological modeling, prompting researchers to explore more complex ecological interactions and enriching our overall understanding of ecosystems.*

5. Numerical simulation

5.1. Numerical simulation without diffusion

In this part, we perform numerical simulations of system (3.2), adjusting the parameter τ based on the theoretical results of Section 3. The selection of parameters for each set of images is shown in Table 1.

Table 1. Parameter selection for numerical simulations in the absence of diffusion.

Number	Figure	τ	β	α	r	k
(1)	Figure 1	1.2	0.5	0.4	0.8	1
(2)	Figures 2 and 3	0.421004	0.89	0.56	0.9	2
(3)	Figures 4 and 5	2.316924	0.77	0.76	0.93	1

(1) When $\tau = 1.2, \beta = 0.5, \alpha = 0.4, r = 0.8, k = 1$, we can calculate that $u^* = 0.64$, $v^* = 0.193109$, $\lambda_1(\tau) = 0.814937 + 0.215692\mathrm{i}$, $\lambda_2(\tau) = 0.814937 - 0.215692\mathrm{i}$, $1 - tr(\tau) + \det(\tau) = 0.080771 > 0$, $1 + tr(\tau) + \det(\tau) = 3.34052 > 0$, $1 - \det(\tau) = 0.289354 > 0$. The parameter set chosen fulfills condition (3.5). According to Theorem 3.3, system (3.2) exhibits local asymptotic stability at the equilibrium point $E^*(u^*, v^*)$, as depicted in Figure 1.

(2) When τ=1.378279274904209, $\beta = 0.79$, $\alpha = 0.56$, $r = 0.99$, $k = 2$, we can calculate that $u^* = 0.502484$, $v^* = 0.236899$, $\lambda_1\left(\tau_1^*\right) = 0.882546 + 0.470226\mathrm{i}$, $\lambda_2\left(\tau_1^*\right) = 0.882546 - 0.470226\mathrm{i}$, $\rho = -0.563247431 \neq 0$, $d = \frac{\partial\left|\lambda_{1,2}(\tau)\right|^2}{\partial\tau}\Big|_{\tau=\tau_1^*} = 0.17043568 \neq 0$, $\frac{\left(-2r\sqrt{u^*}+4r(u^*)^{3/2}+v^*+k(v^*)^2\right)^2}{2\beta u^* v^*\left(kr\sqrt{u^*}-kr(u^*)^{3/2}+(1+kv^*)^2\right)} = 0.23490798 \neq 1, 2$. The parameter set chosen fulfills conditions (3.8), (3.11), (3.12), and (3.20). According to Theorem 3.4, system (3.2) exhibits Neimark-Sacker bifurcation at the equilibrium point $E^*(u^*, v^*)$, as depicted in Figure 2 and 3.

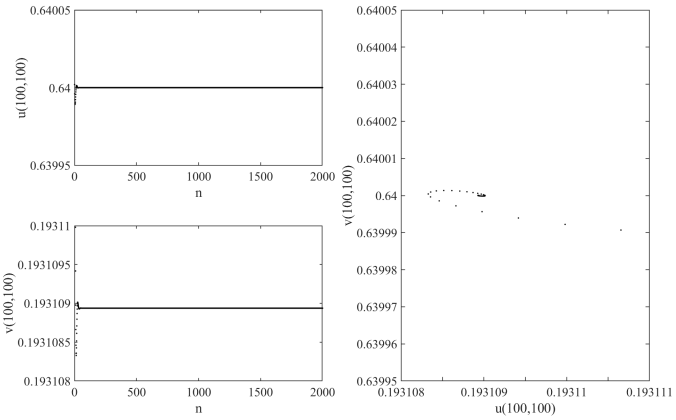

Figure 1. System (3.2) undergos a locally asymptotically stable state for the parameter choices in Table 1 (1).

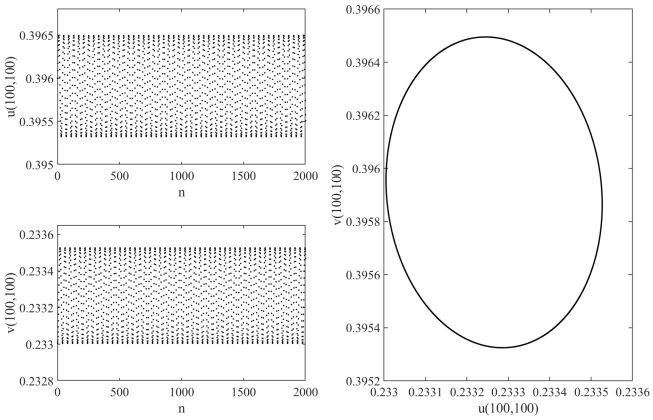

Figure 2. System (3.2) undergos a Neimark-Sacker bifurcation for the parameter choices in Table 1 (2).

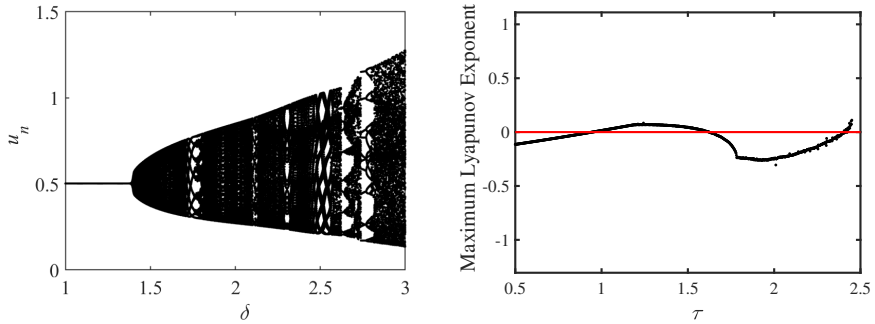

Figure 3. The diagram and MLE of the Neimark-Sacker bifurcation and the value of τ from 1 to 3.

(3) When τ= 2.316924715563065, $\beta = 0.77$, $\alpha = 0.76$, $r = 0.93$, $k = 1$, we can calculate that

$u^* = 0.974194$, $v^* = 0.023151$, $\lambda_1\left(\tau_2^*\right) = -1$, $\lambda_2\left(\tau_2^*\right) = 0.975535$, $\eta_1 = -0.8632132 \neq 0$, $\eta_2 = -190.9651638 \neq 0$. The parameter set chosen fulfills condition (3.22), $\eta_1 \neq 0$, $\eta_2 \neq 0$. According to Theorem 3.5, system (3.2) exhibits Flip bifurcation at the equilibrium point $E^*(u^*, v^*)$, as depicted in Figures 4 and 5.

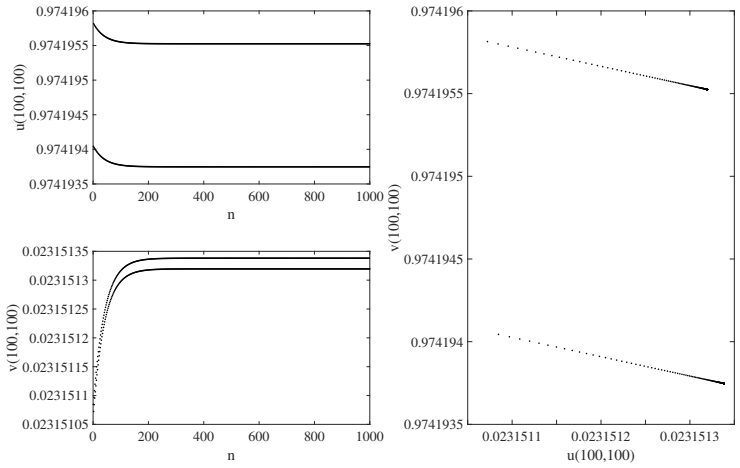

Figure 4. System (3.2) undergos a Flip bifurcation for the parameter choices in Table 1 (3).

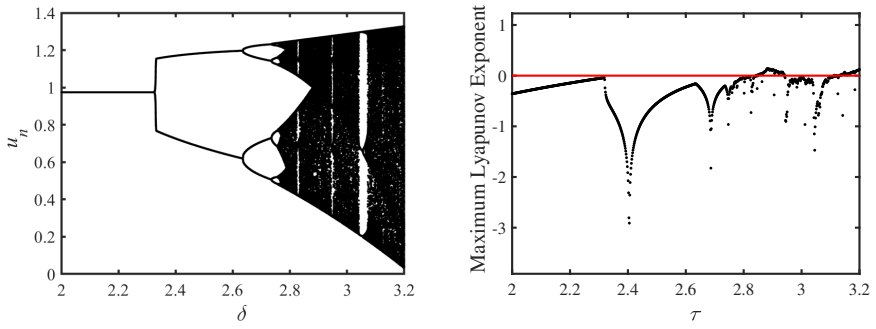

Figure 5. The diagram and MLE of the Flip bifurcation and the value of τ from 2 to 3.2.

5.2. Numerical simulations with spatial inhomogeneity

In accordance with Theorem 4.1, we conducted numerical simulations of systems (2.6) and (2.7). These simulations were performed on a computer with varying parameter values, and the results are presented in Figures 6–49. The values of $u_n(i, j)$ and $v_n(i, j)$ are almost indistinguishable in the visual representations; therefore, we have chosen to display only the relevant images of $u_n(i, j)$. Additionally, we have plotted single-point maps of $u_n(i, j)$ and $v_n(i, j)$ in the two-dimensional space $(m + 2)\times(m + 2)$ at point $(i, j) = \left(\frac{m}{2}, \frac{m}{2}\right)$. For this section, all m values are fixed at 200 and the selected spatial step size is $h = 0.5$. To simplify the characteristic roots, $\lambda_1\left(k_{l,s}^2\right)$ and $\lambda_2\left(k_{l,s}^2\right)$ are expressed in terms of $l_1 = 1$, $s_1 = 1$, $l_2 = 101$, $s_2 = 101$.

5.3. Numerical simulations of self-diffusion

In the case of considering self-diffusion, we let $d_{12} = 0$, $d_{21} = 0$. This means that the main focus is on the spatial distribution and dynamics within the population.

We numerically simulate the system (2.3) with the diffusion coefficient d_{11}, d_{12}, d_{21}, and d_{22} adjusted according to the theoretical results of Section 4. The selection of parameters for each set of images is shown in Table 2–4.

Table 2. Parameter selection for numerical simulations considering self-diffusive states.

	Figure	τ	β	α	r	k	d_{11}	d_{22}
(4)	Figures 6 and 7	1.2	0.5	0.4	0.8	1	0.02	0.051
(5)	Figures 8 and 9	1.2	0.5	0.4	0.8	1	0.02	0.0531
(6)	Figures 10 and 11	1.2	0.5	0.4	0.8	1	0.04	0.001

(4) With the parameters given in Table 2 (4), we can get $\lambda_1\left(k^2_{l_1,s_1}\right) = 0.162158$, $\lambda_2\left(k^2_{l_1,s_1}\right) = -0.97443$, $P_{\max} = \left|\lambda_2\left(k^2_{l_1,s_1}\right)\right| = 0.97443 < 1$, and systems (2.6) and (2.7), with a stable spatially homogeneous stationary state (Figures 6 and 7).

(5) With the parameters given in Table 2 (5), we can get $\lambda_1\left(k^2_{l_2,s_2}\right) = 0.162338$, $\lambda_2\left(k^2_{l_2,s_2}\right) = -1.055247$, $P_{\max} = \left|\lambda_2\left(k^2_{l_2,s_2}\right)\right| = 1.055247 > 1$, and systems (2.6) and (2.7), with pure Turing instability (Figures 8 and 9).

(6) With the parameters given by Table 2 (6), we can get $\lambda_1\left(k^2_{l_2,s_2}\right) = 1.027747$, $\lambda_2\left(k^2_{l_2,s_2}\right) = -0.369199$, $P_{\max} = \left|\lambda_1\left(k^2_{l_2,s_2}\right)\right| = 1.027747 > 1$, and systems (2.6) and (2.7), occurring form pure Turing instability (Figures 10 and 11).

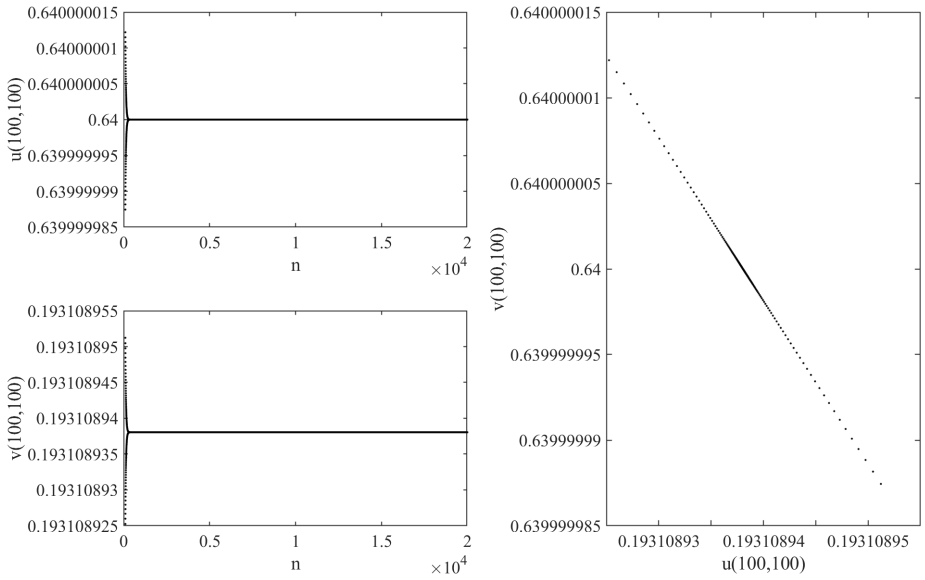

Figure 6. Systems (2.6) and (2.7) undergo a stable spatially homogeneous stationary state for the parameter choices in Table 2 (4).

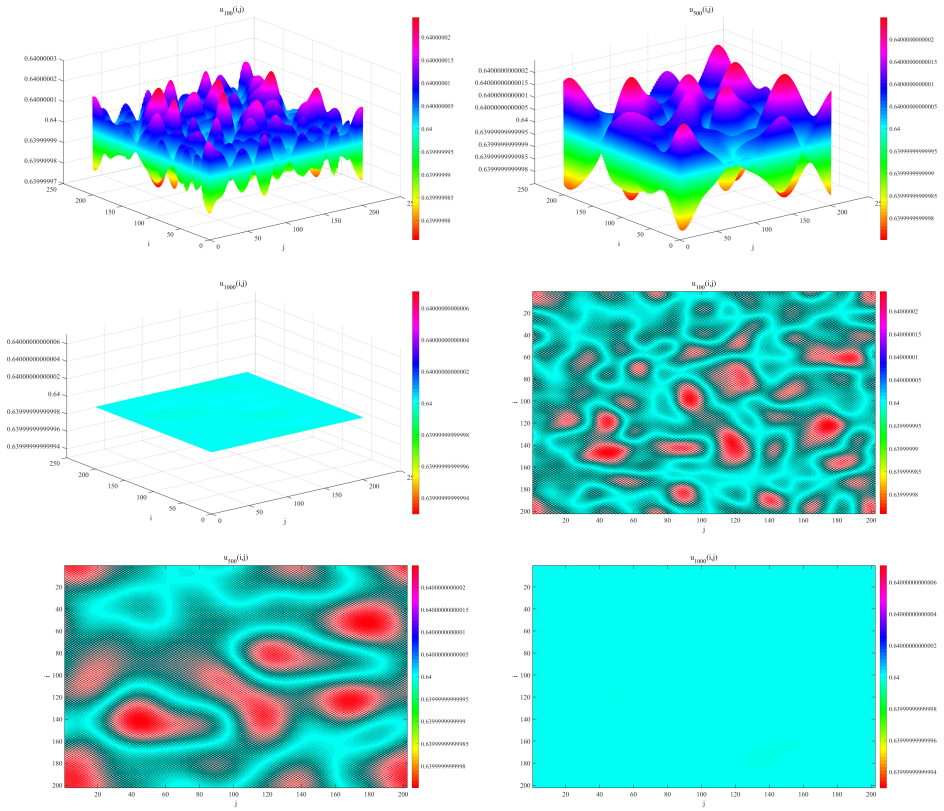

Figure 7. Systems (2.6) and (2.7) undergo a stable spatially homogeneous stationary state.

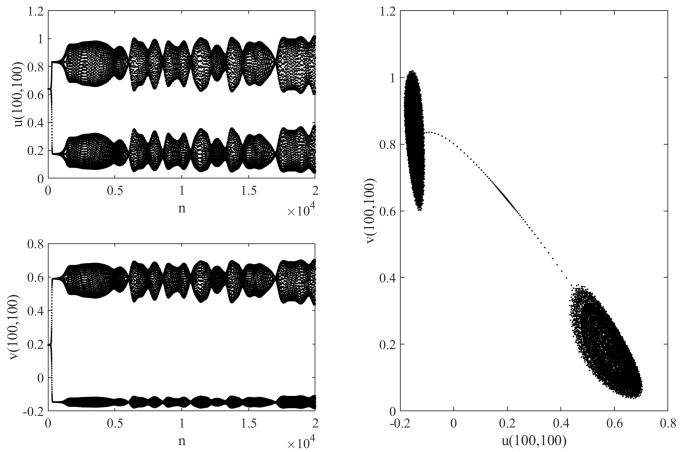

Figure 8. Systems (2.6) and (2.7) undergo pure Turing instability for the parameter choices in Table 2 (5).

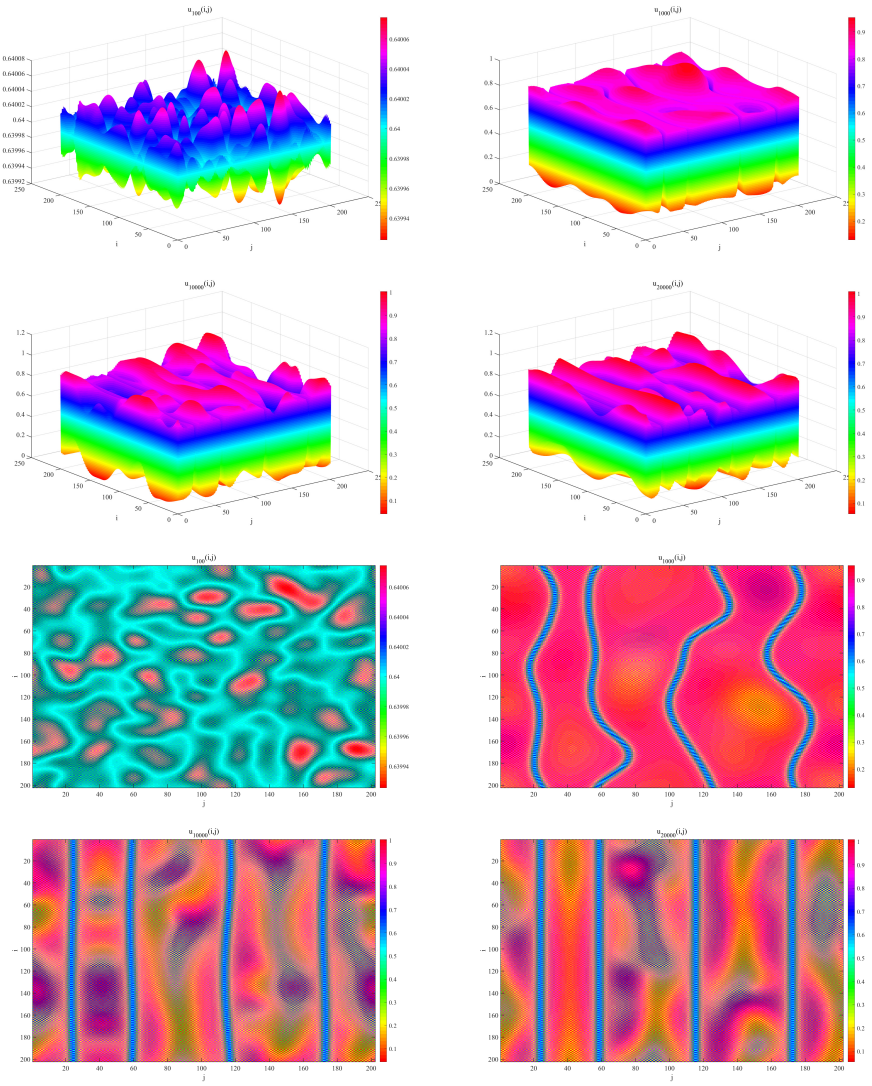

Figure 9. Systems (2.6) and (2.7) undergo pure Turing instability.

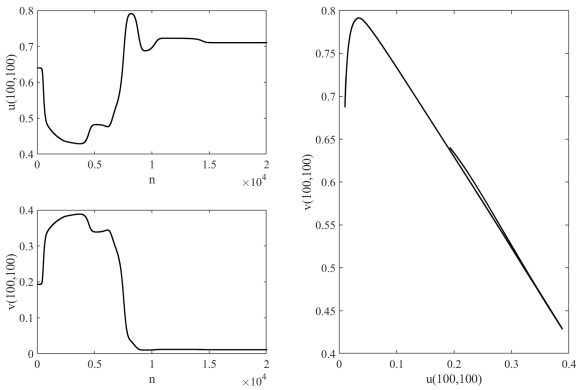

Figure 10. Systems (2.6) and (2.7) undergo pure Turing instability for the parameter choices in Table 2 (6).

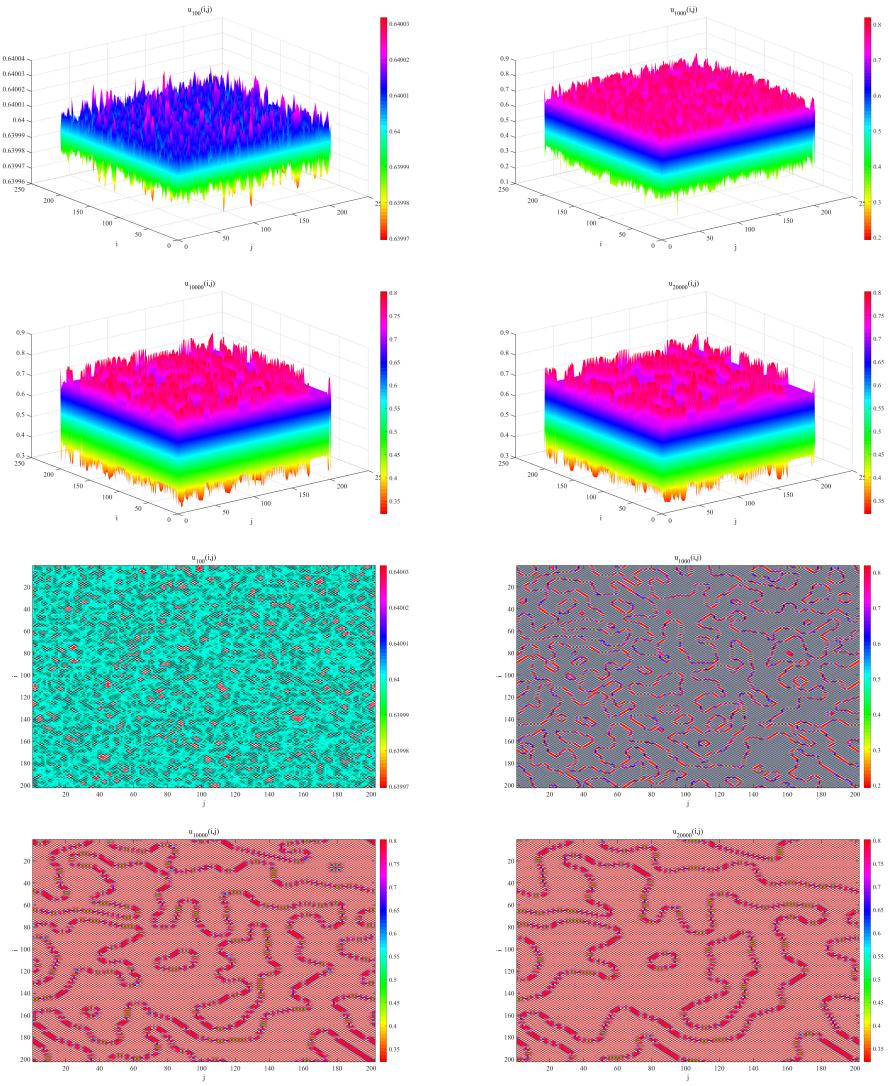

Figure 11. Systems (2.6) and (2.7) undergo pure Turing instability.

Table 3. Parameter selection for numerical simulations considering self-diffusive states.

	Figure	τ	β	α	r	k	d_{11}	d_{22}
(7)	Figures 12 and 13	0.421004	0.89	0.56	0.9	2	0.08	0.04
(8)	Figures 14 and 15	0.421004	0.89	0.56	0.9	2	0.14	0.1576
(9)	Figures 16 and 17	0.421004	0.89	0.56	0.9	2	0.15	0.060194
(10)	Figures 18 and 19	0.421004	0.89	0.56	0.9	2	0.14	0.1585

(7) With the parameters given by Table 3 (7), we can get $\lambda_1\left(k^2_{l_1,s_1}\right) = 0.188382$, $\lambda_2\left(k^2_{l_1,s_1}\right) = -0.079129$, $P_{\max} = \left|\lambda_1\left(k^2_{l_1,s_1}\right)\right| = 0.188382 < 1$, systems (2.6) and (2.7), which exhibit a stable spatially homogeneous stationary state (Figures 12 and 13).

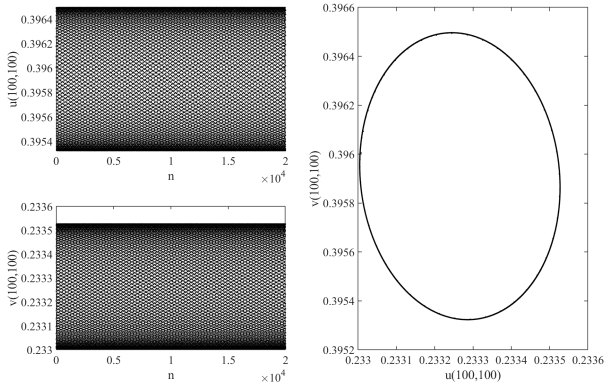

Figure 12. Systems (2.6) and (2.7) undergo a stable spatially homogeneous stationary state for the parameter choices in Table 3 (7).

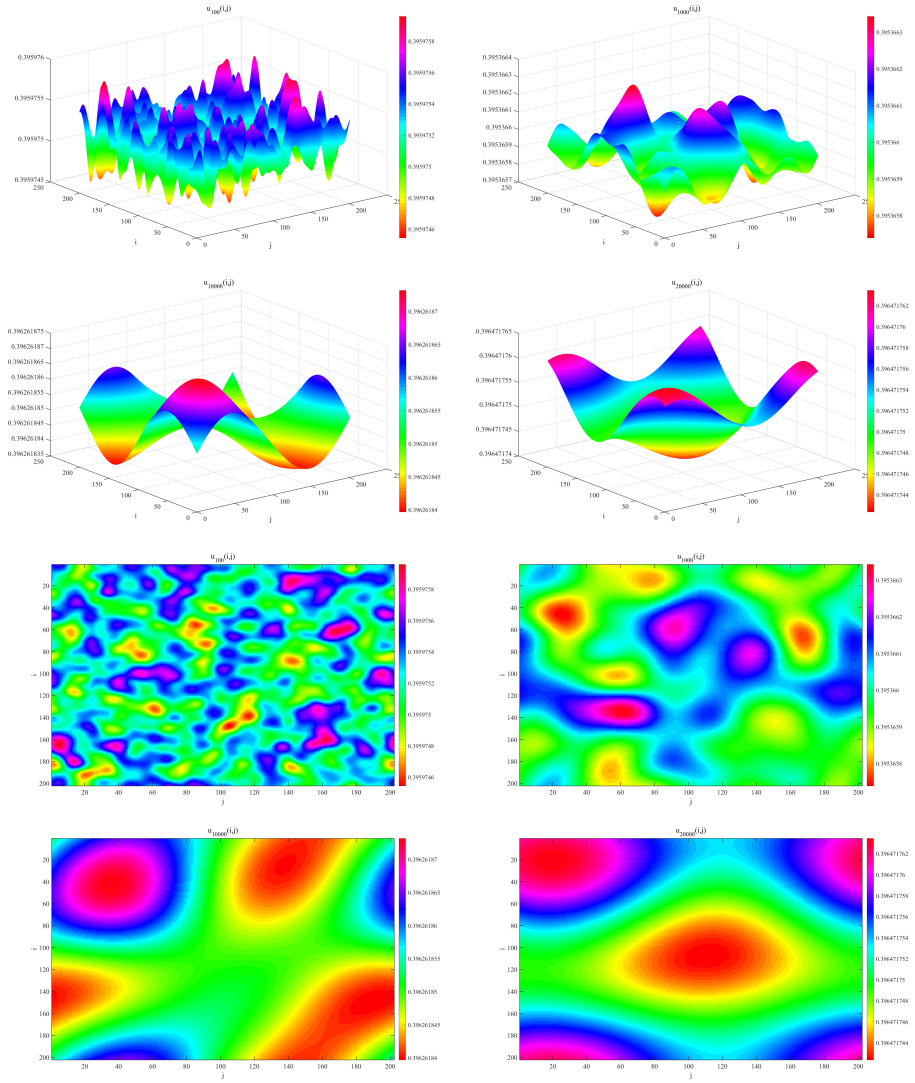

Figure 13. Systems (2.6) and (2.7) undergo a stable spatially homogeneous stationary state.

(8) With the parameters given by Table 3 (8), we can get $\lambda_1\left(k^2_{l_1,s_1}\right) = -0.99391 + 0.086131\text{i}$, $\lambda_2\left(k^2_{l_1,s_1}\right) = -0.99391 - 0.086131\text{i}$, $P_{\max} = \left|\lambda_{1,2}\left(k^2_{l_1,s_1}\right)\right| = 1$, systems (2.6) and (2.7), which exhibit a Neimark-Sacker-Neimark-Sacker (Figures 14 and 15).

(9) With the parameters given by Table 3 (9), we can get $\lambda_1\left(k^2_{l_1,s_1}\right) = 0.192995$, $\lambda_2\left(k^2_{l_1,s_1}\right) = -1$, $P_{\max} = \left|\lambda_2\left(k^2_{l_1,s_1}\right)\right| = 1$, where systems (2.6) and (2.7) exhibit a Neimark-Sacker-Flip (Figures 16 and 17).

(10) With the parameters given by Table 3 (10), we can get $\lambda_1\left(k^2_{l_2,s_2}\right) = -0.999971 + 0.07794\text{i}$, $\lambda_2\left(k^2_{l_2,s_2}\right) = -0.999971 - 0.07794\text{i}$, $P_{\max} = \left|\lambda_{1,2}\left(k^2_{l_2,s_2}\right)\right| = 1.077911 > 1$, where systems (2.6) and (2.7) exhibit Neimark-Sacker-Turing instability (Figures 18 and 19).

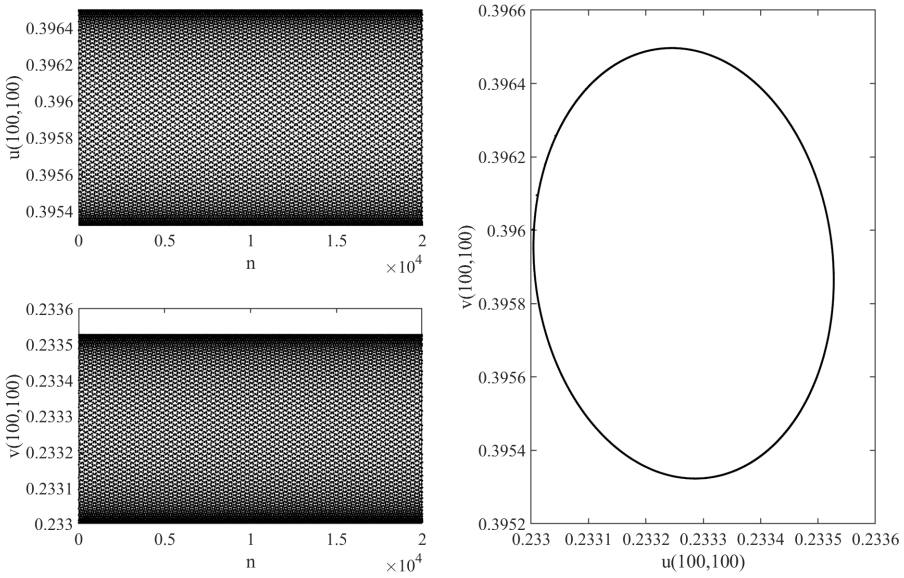

Figure 14. Systems (2.6) and (2.7) undergo a Neimark-Sacker-Neimark-Sacker bifurcation for the parameter choices in Table 3 (8).

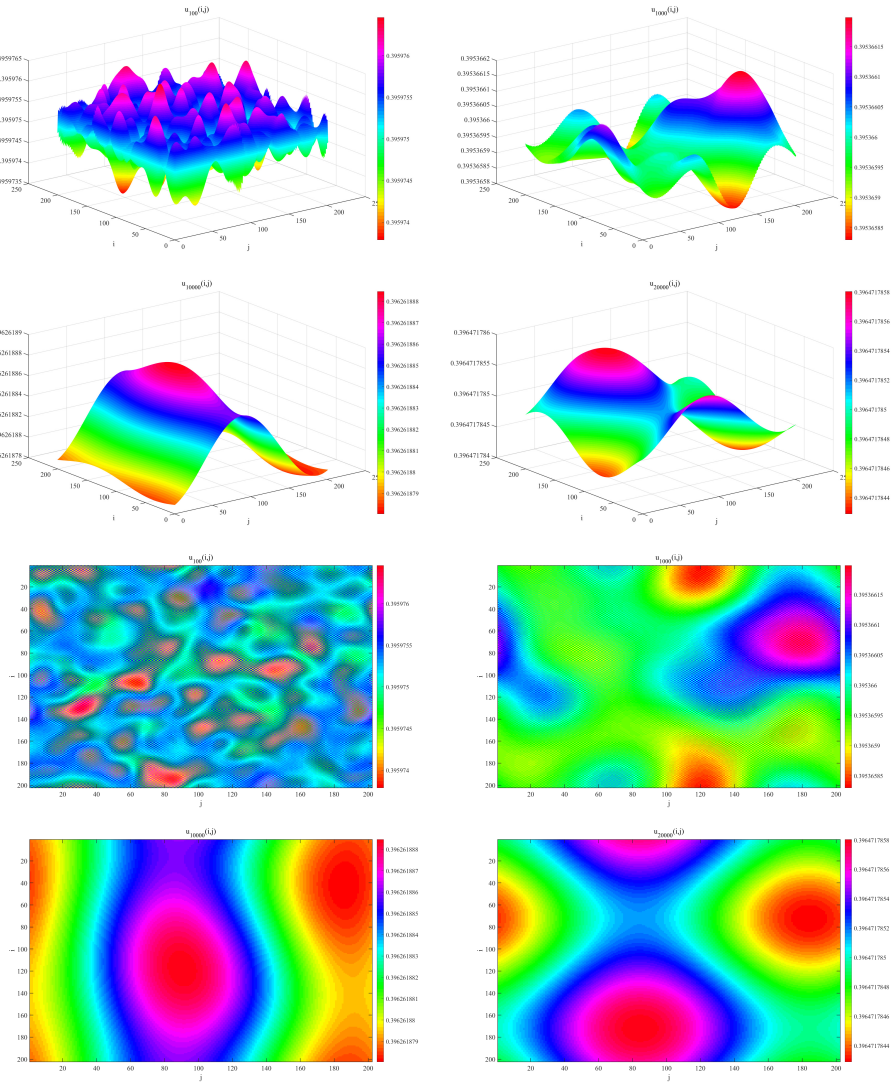

Figure 15. Systems (2.6) and (2.7) undergo a Neimark-Sacker-Neimark-Sacker bifurcation.

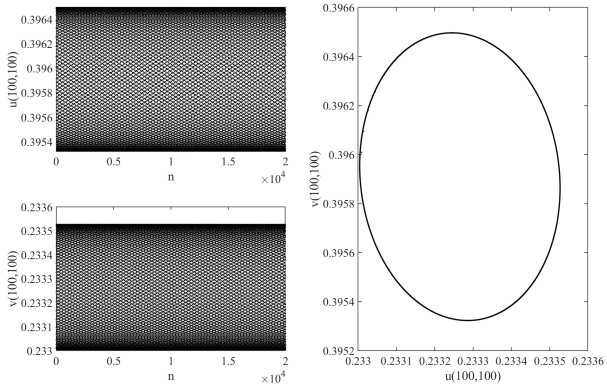

Figure 16. Systems (2.6) and (2.7) undergo a Neimark-Sacker-Flip bifurcation for the parameter choices in Table 3 (9).

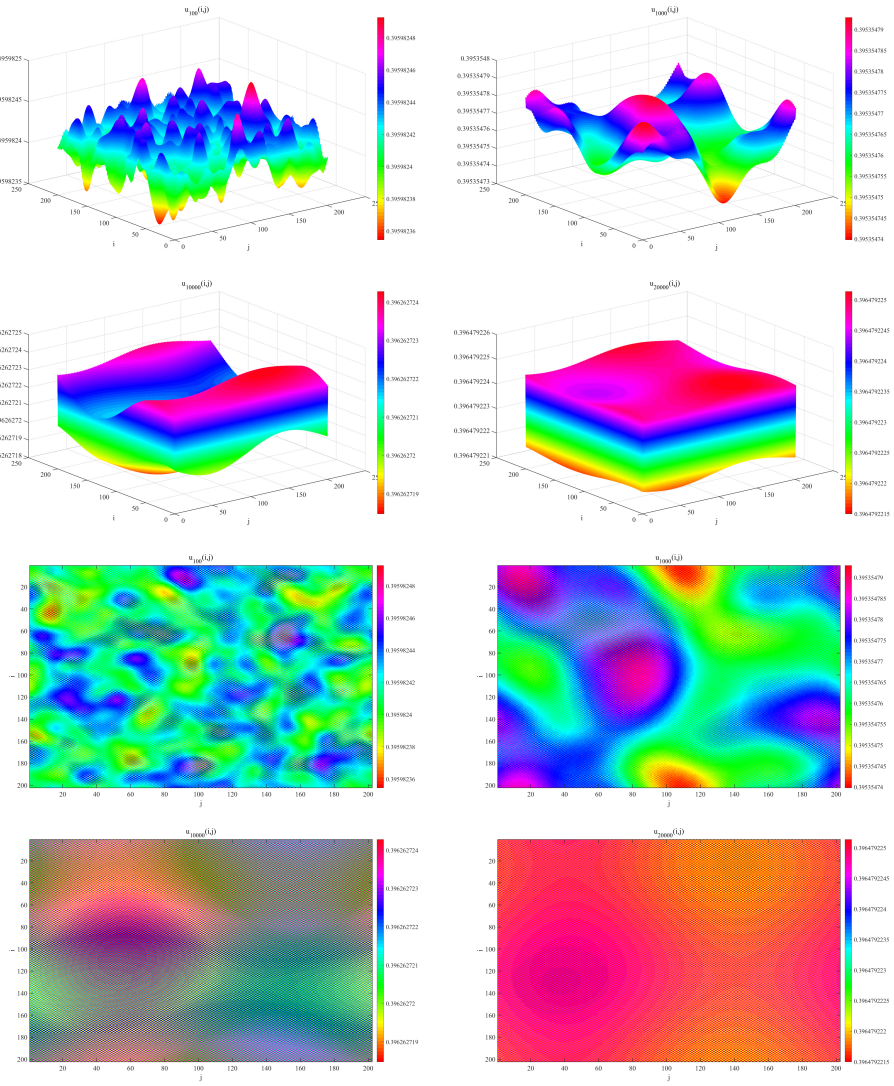

Figure 17. Systems (2.6) and (2.7) undergo a Neimark-Sacker-Flip bifurcation.

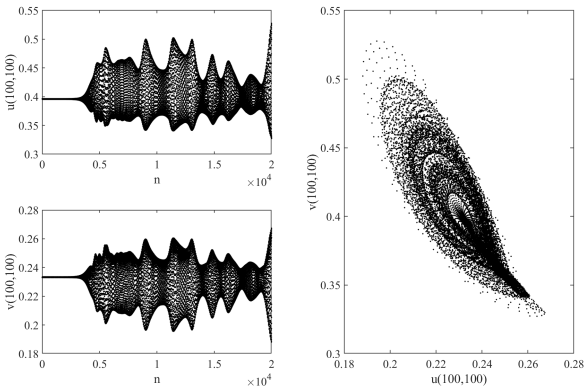

Figure 18. Systems (2.6) and (2.7) undergo Neimark-Sacker-Turing instability for the parameter choices in Table 3 (10).

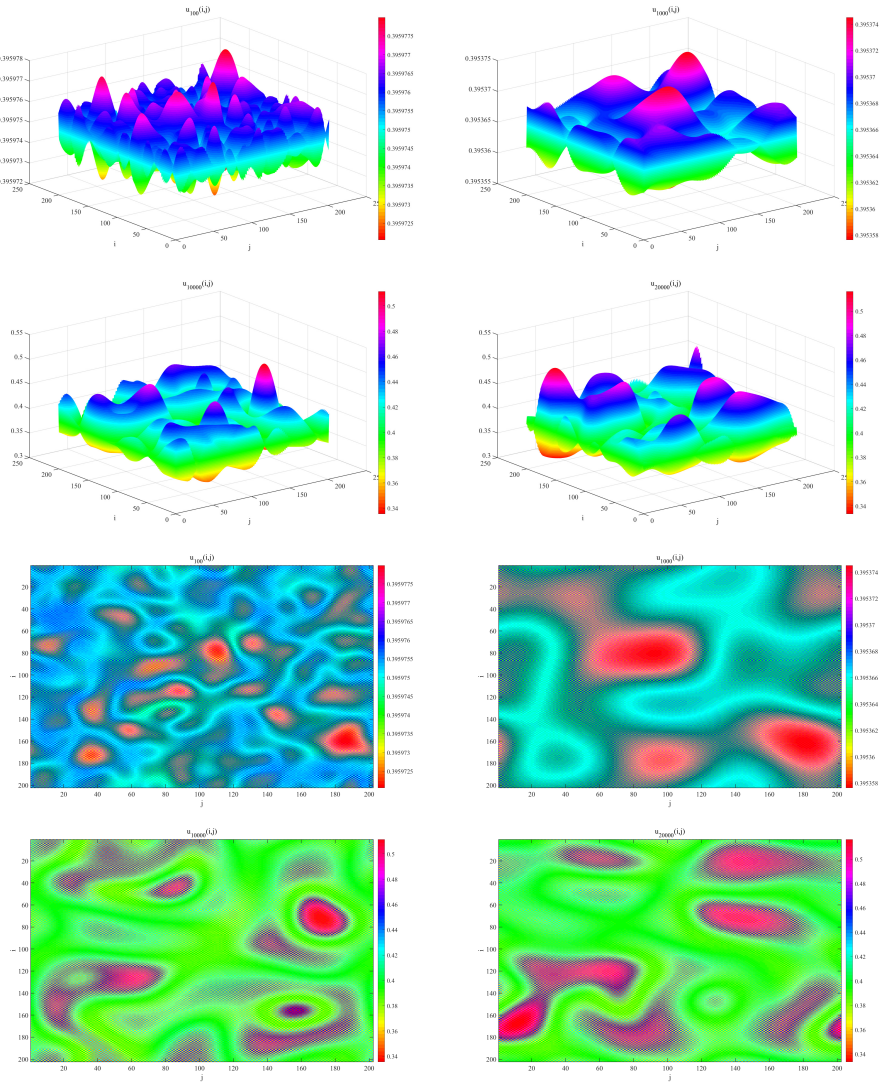

Figure 19. Systems (2.6) and (2.7) undergo Neimark-Sacker-Turing instability.

Table 4. Parameter selection for numerical simulations considering self-diffusive states.

	Figure	τ	β	α	r	k	d_{11}	d_{22}
(11)	Figures 20 and 21	2.316924	0.77	0.76	0.93	1	0.02	0.0256
(12)	Figures 22 and 23	1.2	0.5	0.4	0.8	1	0.02	0.051774409
(13)	Figures 24 and 25	2.316924	0.77	0.76	0.93	1	0.01	0.02674
(14)	Figures 26 and 27	2.316924	0.77	0.76	0.93	1	0.01	0.0272

(11) With the parameters given by Table 4 (11), we can get $\lambda_1\left(k^2_{l_1,s_1}\right) = 0.478856$, $\lambda_2\left(k^2_{l_1,s_1}\right) = -0.948964$, $P_{\max} = \left|\lambda_2\left(k^2_{l_1,s_1}\right)\right| = 0.948964 < 1$, where systems (2.6) and (2.7) exhibit a stable spatially homogeneous stationary state (Figures 20 and 21).

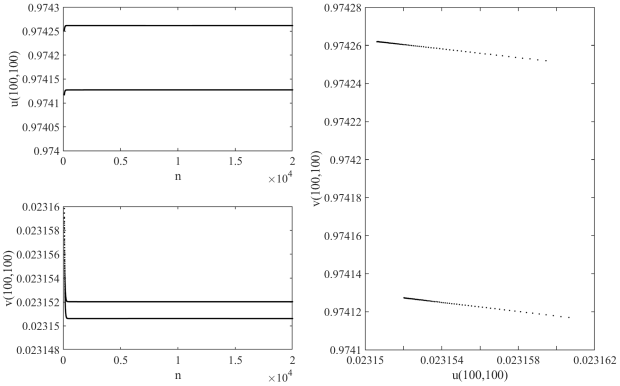

Figure 20. Systems (2.6) and (2.7) undergo a stable spatially homogeneous stationary state for the parameter choices in Table 4 (11).

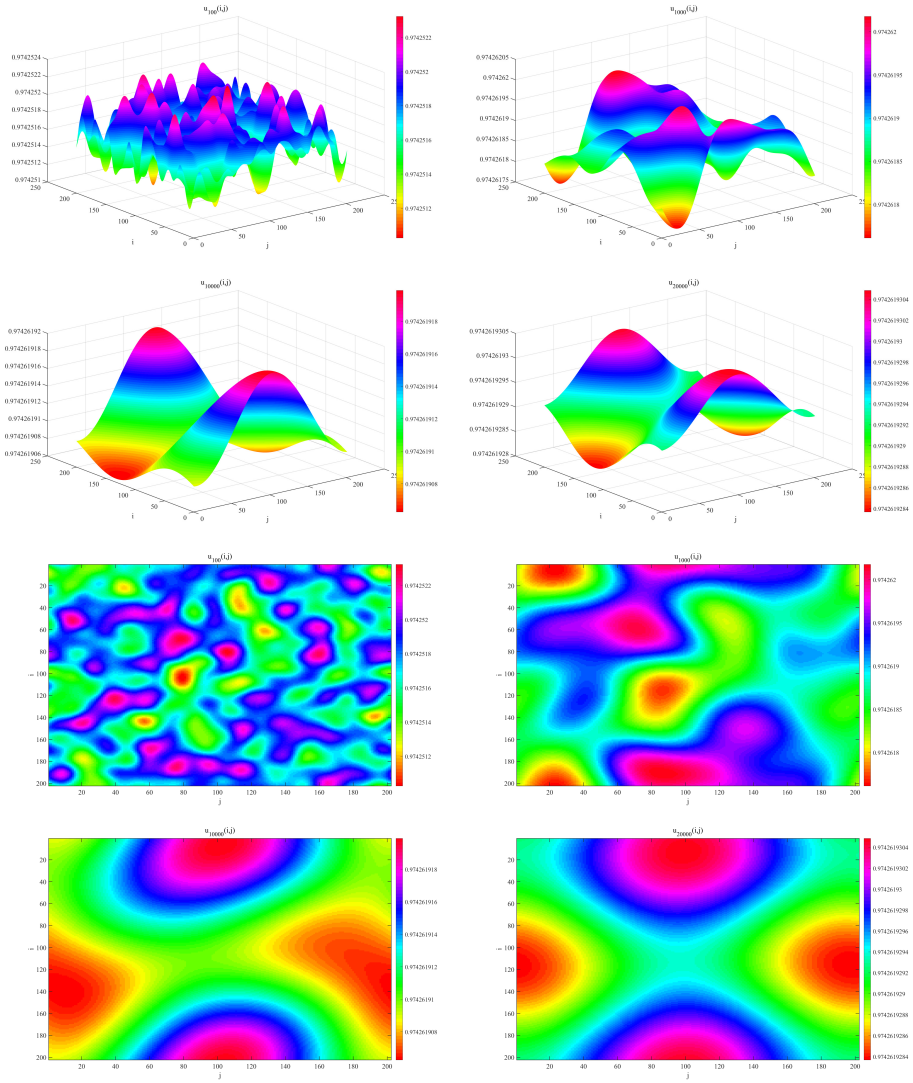

Figure 21. Systems (2.6) and (2.7) undergo a stable spatially homogeneous stationary state.

(12) With the parameters given by Table 4 (12), we can get $\lambda_1\left(k^2_{l_1,s_1}\right) = 0.162218$, $\lambda_2\left(k^2_{l_1,s_1}\right) = -1$, $P_{\max} = \left|\lambda_2\left(k^2_{l_1,s_1}\right)\right| = 1$, where systems (2.6) and (2.7) exhibit Flip bifurcation (Figures 22 and 23).

(13) With the parameters given by Table 4 (13), we can get $\lambda_1\left(k^2_{l_1,s_1}\right) = -0.247986$, $\lambda_2\left(k^2_{l_1,s_1}\right) = -1$, $P_{\max} = \left|\lambda_2\left(k^2_{l_1,s_1}\right)\right| = 1$, where systems (2.6) and (2.7) exhibit a Flip-Flip bifurcation (Figures 24 and 25).

(14) With the parameters given by Table 4 (14), we can get $\lambda_1\left(k^2_{l_2,s_2}\right) = -0.248172$, $\lambda_2\left(k^2_{l_2,s_2}\right) = -1.03339$, $P_{\max} = \left|\lambda_2\left(k^2_{l_2,s_2}\right)\right| = 1.03339 > 1$, where systems (2.6) and (2.7) exhibit Flip-Turing instability (Figures 26 and 27).

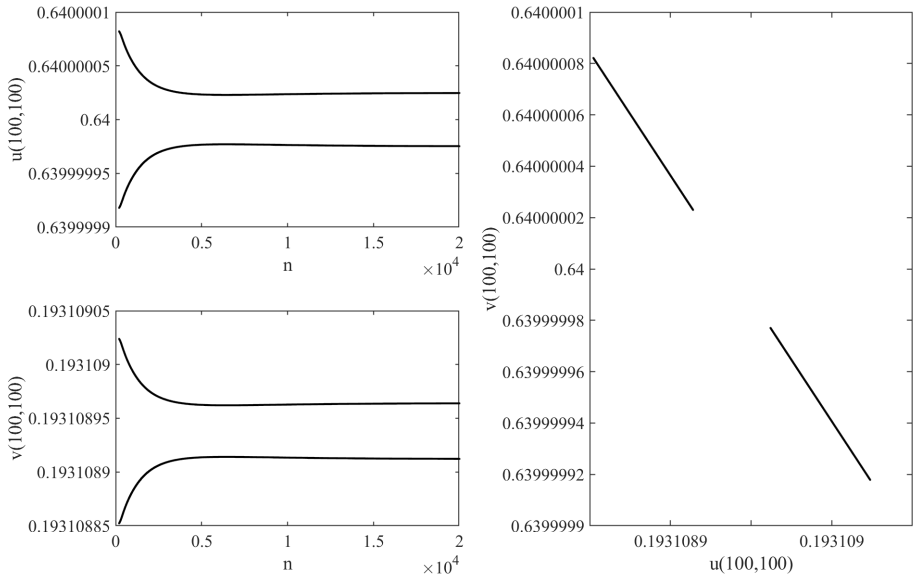

Figure 22. Systems (2.6) and (2.7) undergo a Flip bifurcation for the parameter choices in Table 4 (12).

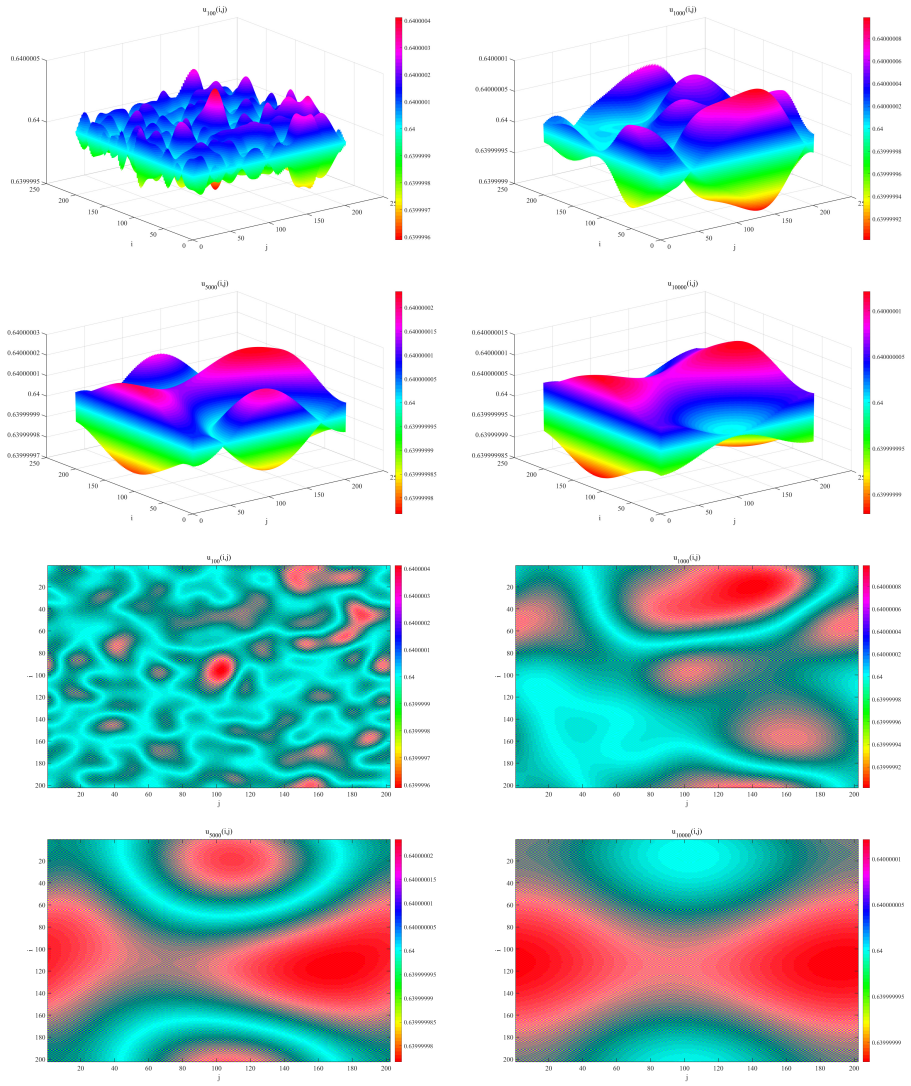

Figure 23. Systems (2.6) and (2.7) undergo a Flip bifurcation.

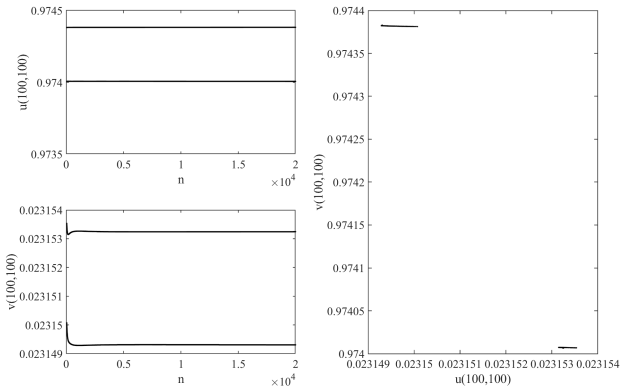

Figure 24. Systems (2.6) and (2.7) undergo a Flip-Flip bifurcation for the parameter choices in Table 4 (13).

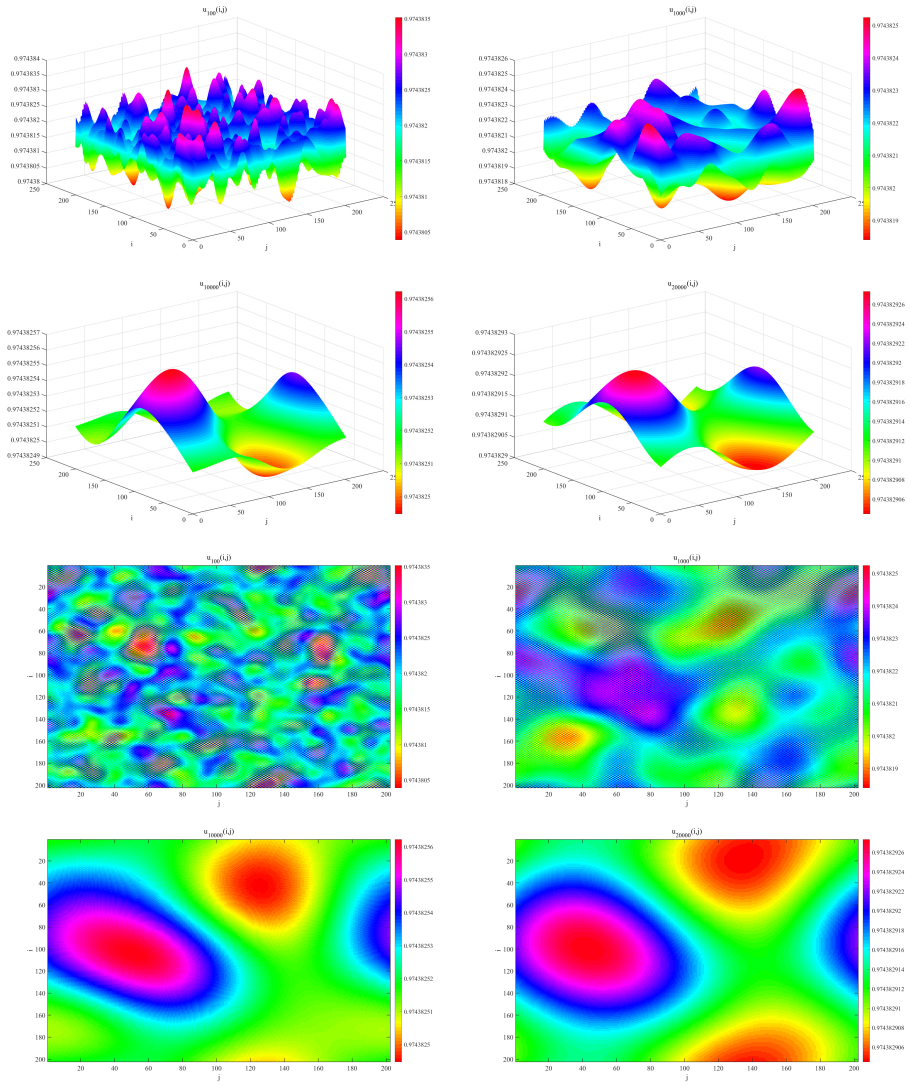

Figure 25. Systems (2.6) and (2.7) undergo a Flip-Flip bifurcation.

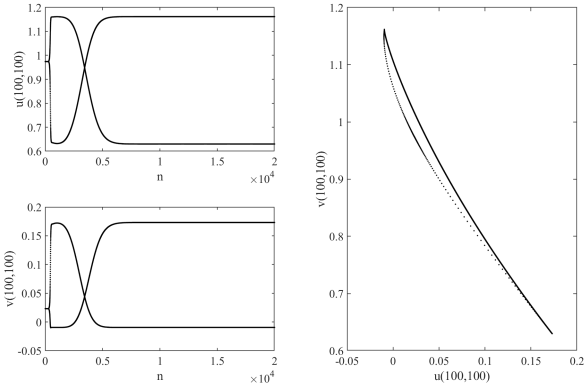

Figure 26. Systems (2.6) and (2.7) undergo Flip-Turing instability for the parameter choices in Table 4 (14).

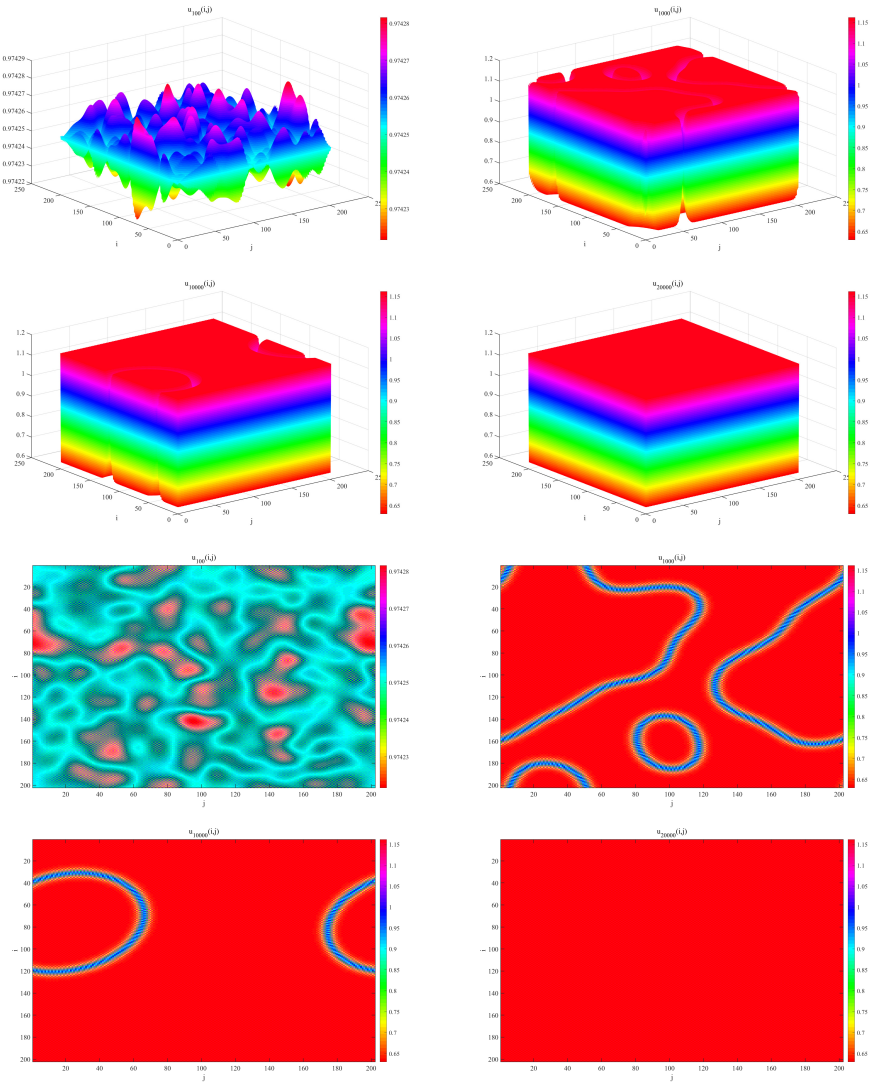

Figure 27. Systems (2.6) and (2.7) undergo Flip-Turing instability.

5.4. Numerical simulations of cross-diffusion

Cross-diffusion serves as a powerful tool in elucidating the spatial propagation of predator-prey interactions, offering a more precise portrayal of their distribution and interplay in space. By incorporating cross-diffusion, the model becomes adept at capturing the intricate spatial dynamics between predator and prey populations, thereby enhancing its ability to forecast their behavior and evolutionary trajectories within the ecosystem.

We numerically simulate the system (2.3) with the diffusion coefficient d_{11}, d_{12}, d_{21}, and d_{22} adjusted according to the theoretical results of Section 4. The selection of parameters for each set of images is shown in Table 5–7.

Table 5. Parameter selection for numerical simulations considering cross-diffusion states.

	Figure	τ	β	α	r	k	d_{11}	d_{12}	d_{21}	d_{22}
(15)	Figures 28 and 29	1.2	0.5	0.4	0.8	1	0.04	0.01	0.01	0.066
(16)	Figures 30 and 31	1.2	0.5	0.4	0.8	1	0.02	0.01	0.01	0.0586
(17)	Figures 32 and 33	1.2	0.5	0.4	0.8	1	0.004	0.01	0.01	0.028

(15) With the parameters given by Table 2 (4), we can get $\lambda_1\left(k^2_{l_1,s_1}\right) = -0.487432$, $\lambda_2\left(k^2_{l_1,s_1}\right) = -0.984083$, $P_{\max} = \left|\lambda_2\left(k^2_{l_1,s_1}\right)\right| = 0.984083 < 1$, where systems (2.6) and (2.7) exhibit a stable spatially homogeneous stationary state (Figures 28 and 29).

(16) With the parameters given by Table 2 (5), we can get $\lambda_1\left(k^2_{l_2,s_2}\right) = 0.307499$, $\lambda_2\left(k^2_{l_2,s_2}\right) = -1.011111$, $P_{\max} = \left|\lambda_2\left(k^2_{l_2,s_2}\right)\right| = 1.011111 > 1$, where systems (2.6) and (2.7) exhibit pure Turing instability (Figures 30 and 31).

(17) With the parameters given by Table 2 (6), we can get $\lambda_1\left(k^2_{l_2,s_2}\right) = 1.00735$, $\lambda_2\left(k^2_{l_2,s_2}\right) = -0.148926$, $P_{\max} = \left|\lambda_2\left(k^2_{l_2,s_2}\right)\right| = 1.00735 > 1$, where systems (2.6) and (2.7) exhibit pure Turing instability (Figures 32 and 33).

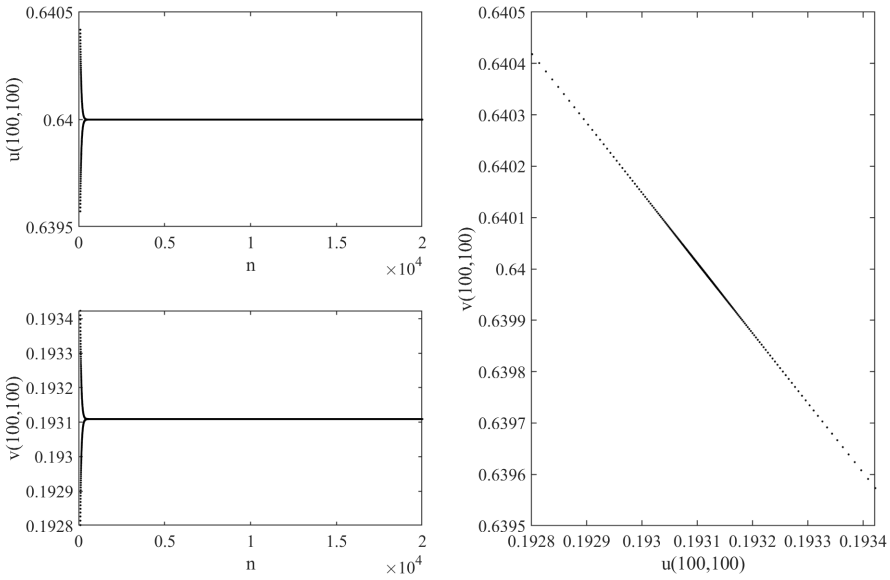

Figure 28. Systems (2.6) and (2.7) undergo a stable spatially homogeneous stationary state for the parameter choices in Table 5 (15).

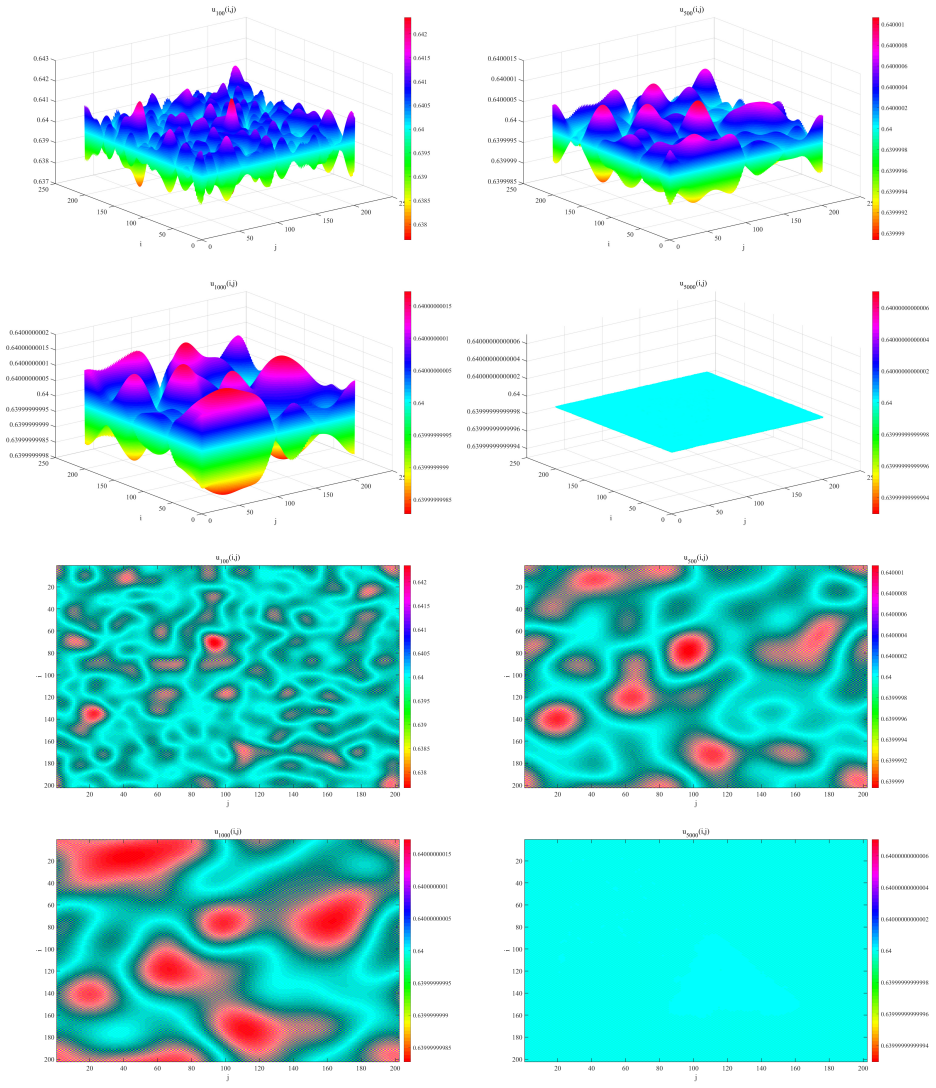

Figure 29. Systems (2.6) and (2.7) undergo a stable spatially homogeneous stationary state.

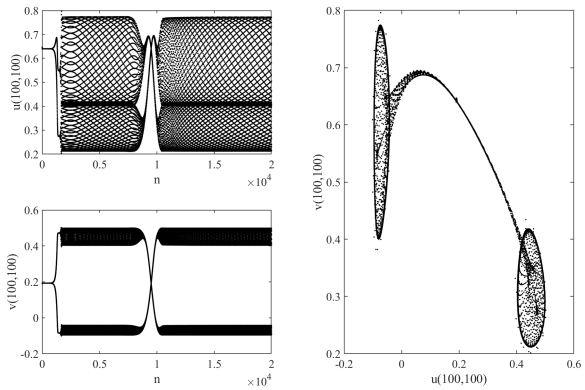

Figure 30. Systems (2.6) and (2.7) undergo pure Turing instability for the parameter choices in Table 5 (16).

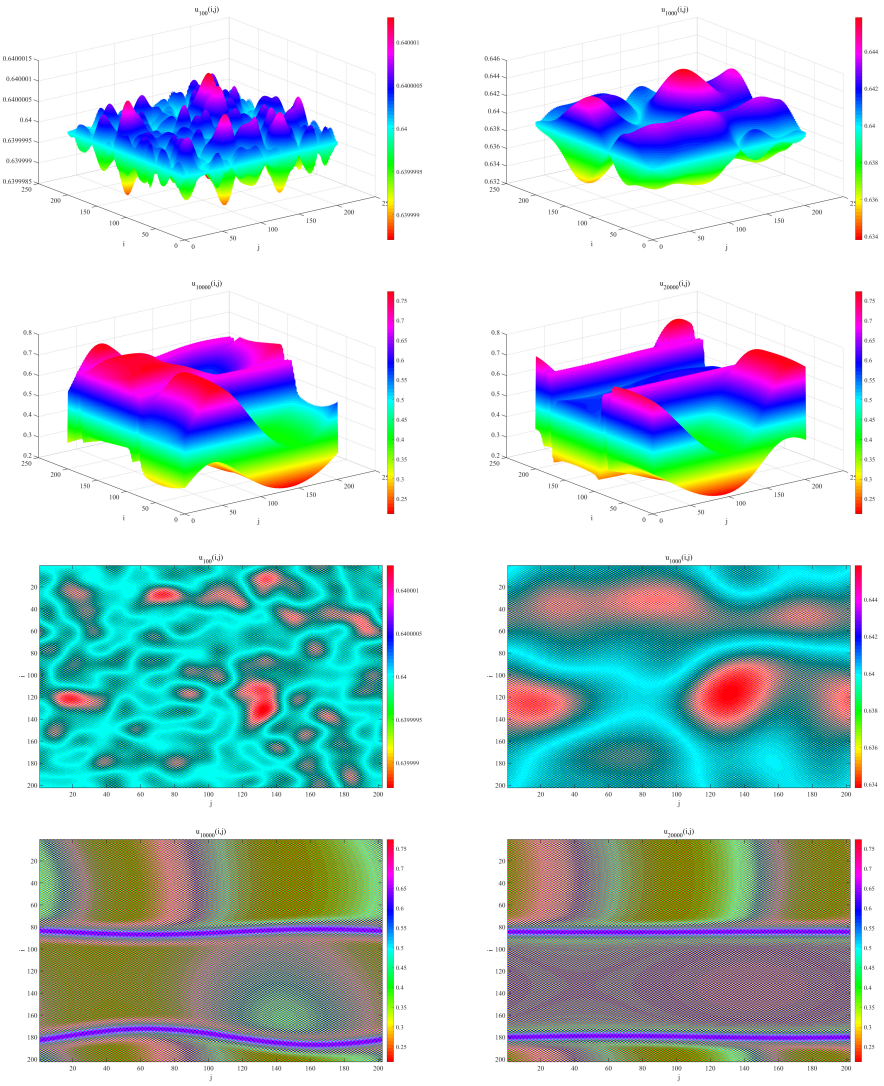

Figure 31. Systems (2.6) and (2.7) undergo pure Turing instability.

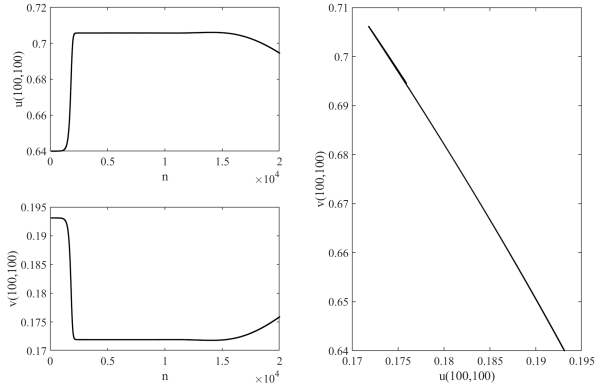

Figure 32. Systems (2.6) and (2.7) undergo pure Turing instability for the parameter choices in Table 5 (17).

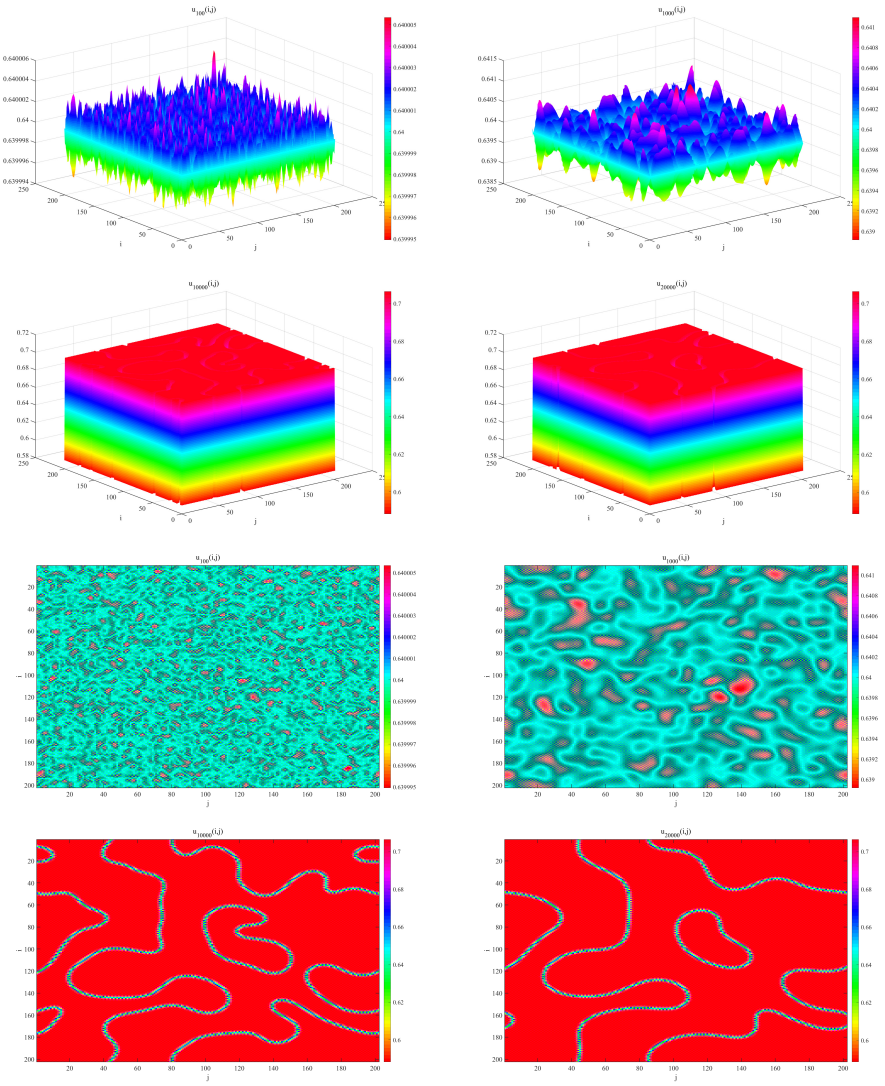

Figure 33. Systems (2.6) and (2.7) undergo pure Turing instability.

Table 6. Parameter selection for numerical simulations considering cross-diffusion states.

	Figure	τ	β	α	r	k	d_{11}	d_{12}	d_{21}	d_{22}
(18)	Figures 34 and 35	0.421004	0.89	0.56	0.9	2	0.1	0.01	0.01	0.15
(19)	Figures 36 and 37	0.421004	0.89	0.56	0.9	2	0.14	0.01	0.01	0.15946
(20)	Figures 38 and 39	0.421004	0.89	0.56	0.9	2	0.1	0.01	0.01	0.15163
(21)	Figures 40 and 41	0.421004	0.89	0.56	0.9	2	0.14	0.01	0.01	0.161

(18) With the parameters given by Table 3 (7), we can get $\lambda_1\left(k^2_{l_1,s_1}\right) = -0.343818$, $\lambda_2\left(k^2_{l_1,s_1}\right) = -0.97811$, $P_{\max} = \left|\lambda_2\left(k^2_{l_1,s_1}\right)\right| = 0.97811 < 1$, where systems (2.6) and (2.7) exhibit a stable spatially homogeneous stationary state (Figures 34 and 35).

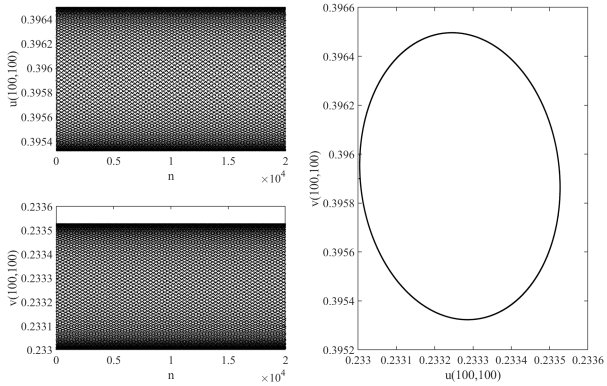

Figure 34. Systems (2.6) and (2.7) undergo a stable spatially homogeneous stationary state for the parameter choices in Table 6 (18).

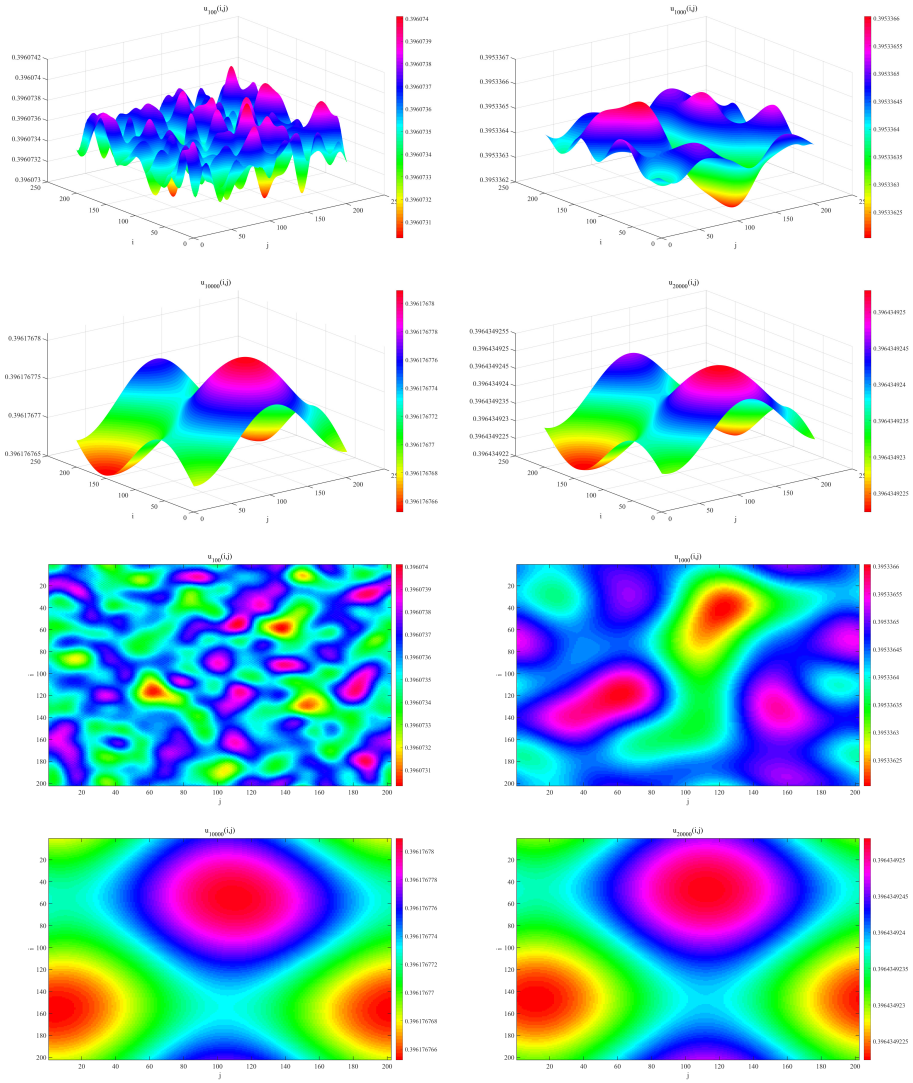

Figure 35. Systems (2.6) and (2.7) undergo a stable spatially uniform steady state.

(19) With the parameters given by Table 3 (8), we can get $\lambda_1\left(k^2_{l_1,s_1}\right) = -0.987596 + 0.15486\mathrm{i}$, $\lambda_2\left(k^2_{l_1,s_1}\right) = -0.987596 - 0.15486\mathrm{i}$, $P_{\max} = \left|\lambda_{1,2}\left(k^2_{l_1,s_1}\right)\right| = 1$, where systems (2.6) and (2.7) exhibit a Neimark-Sacker-Neimark-Sacker (Figures 36 and 37).

(20) With the parameters given by Table 3 (9), we can get $\lambda_1\left(k^2_{l_1,s_1}\right) = -0.343932$, $\lambda_2\left(k^2_{l_1,s_1}\right) = -1$, $P_{\max} = \left|\lambda_2\left(k^2_{l_1,s_1}\right)\right| = 1$, where systems (2.6) and (2.7) exhibit a Neimark-Sacker-Flip (Figures 38 and 39).

(21) With the parameters given by Table 3 (10), we can get $\lambda_1\left(k^2_{l_2,s_2}\right) = -0.897022 + 0.483603\mathrm{i}$, $\lambda_2\left(k^2_{l_2,s_2}\right) = -0.897022 - 0.483603\mathrm{i}$, $P_{\max} = \left|\lambda_2\left(k^2_{l_2,s_2}\right)\right| = 1.008817 > 1$, where systems (2.6) and (2.7) exhibit Neimark-Sacker-Turing instability (Figures 40 and 41).

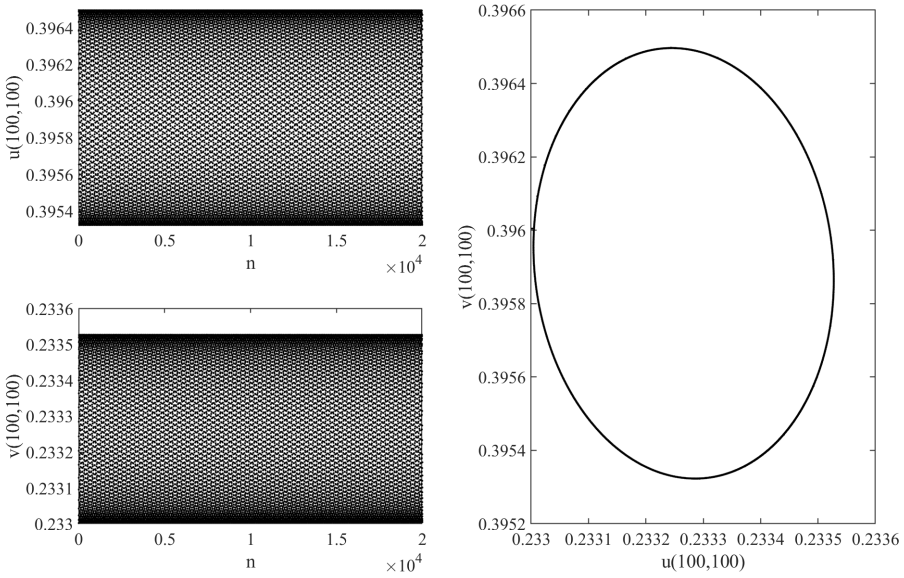

Figure 36. Systems (2.6) and (2.7) undergo a Neimark-Sacker-Neimark-Sacker bifurcation for the parameter choices in Table 6 (19).

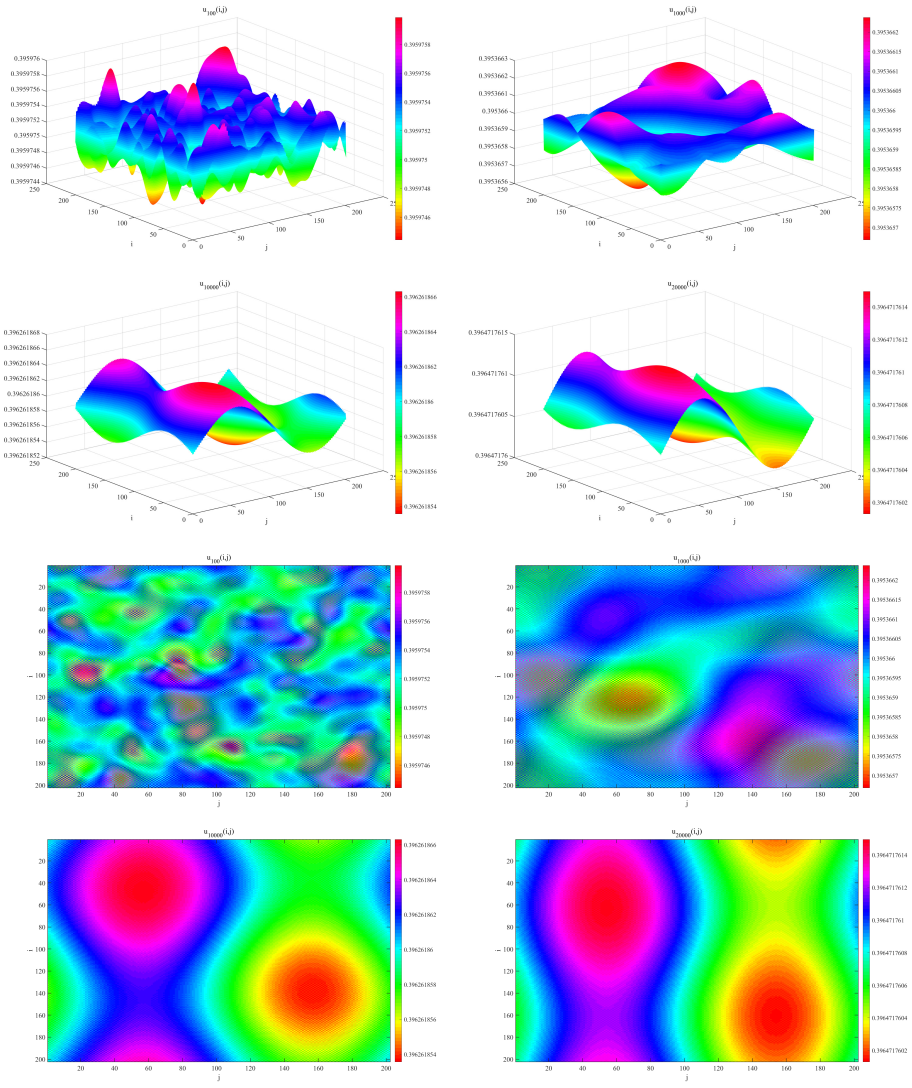

Figure 37. Systems (2.6) and (2.7) undergo a Neimark-Sacker-Neimark-Sacker bifurcation.

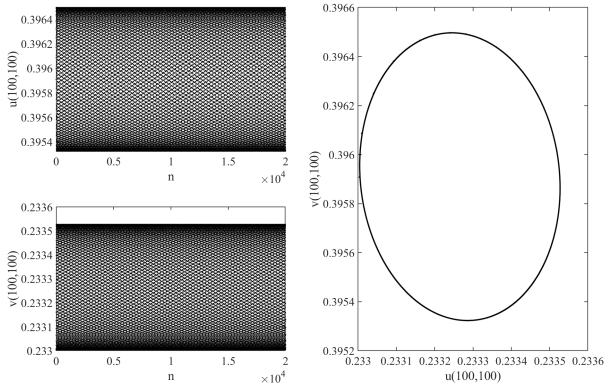

Figure 38. Systems (2.6) and (2.7) undergo a Neimark-Sacker-Flip bifurcation for the parameter choices in Table 6 (20).

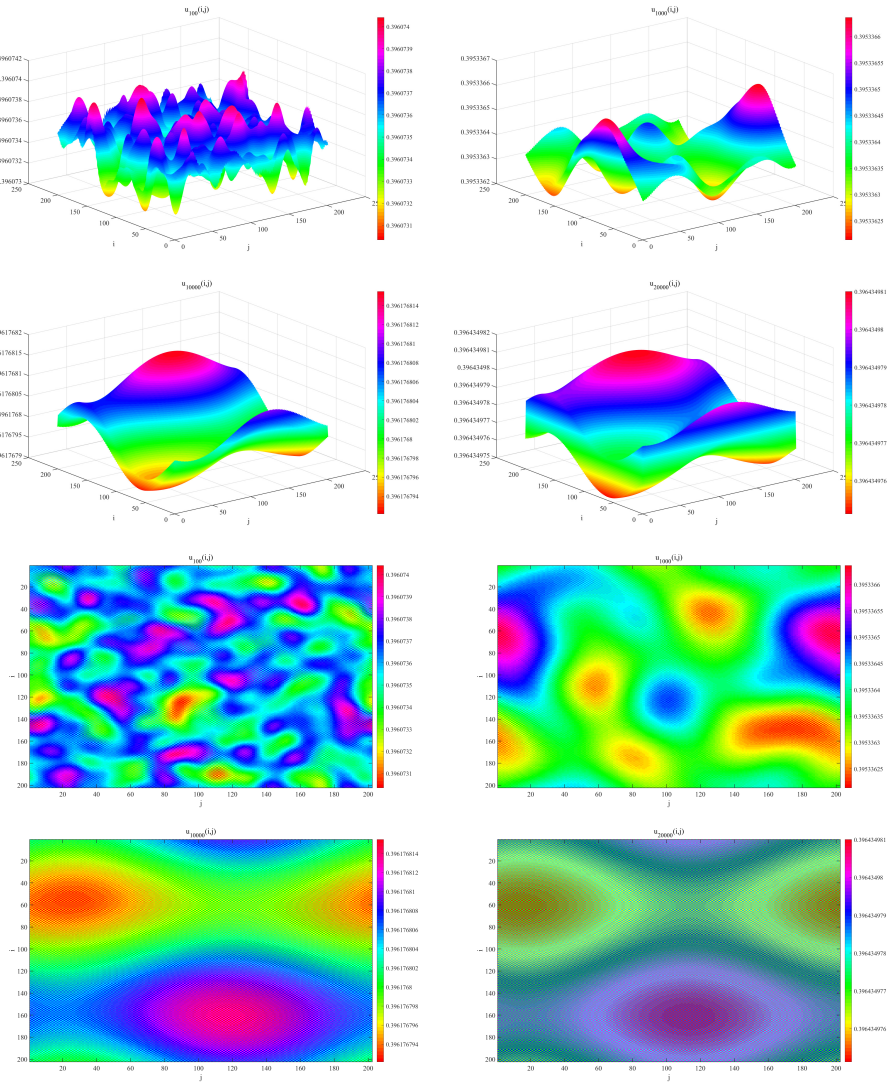

Figure 39. Systems (2.6) and (2.7) undergo a Neimark-Sacker-Flip bifurcation.

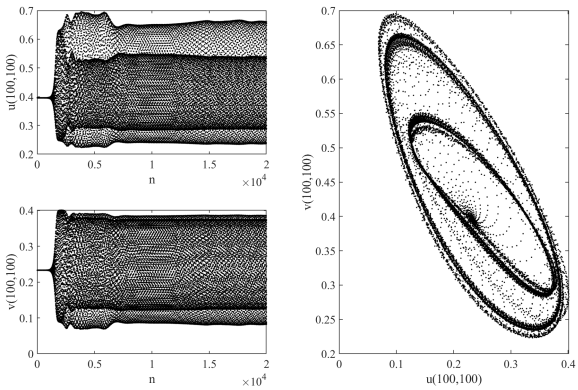

Figure 40. Systems (2.6) and (2.7) undergo Neimark-Sacker-Turing instability for the parameter choices in Table 6 (21).

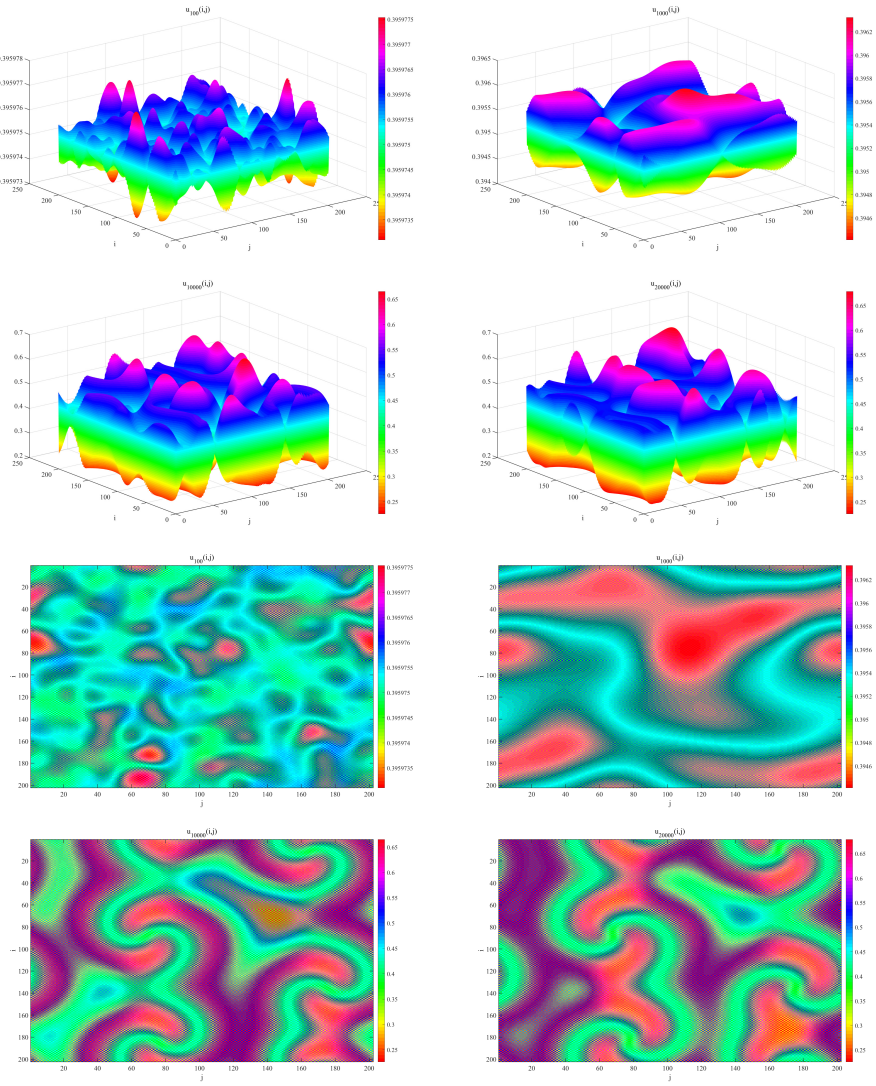

Figure 41. Systems (2.6) and (2.7) undergo Neimark-Sacker-Turing instability.

Table 7. Parameter selection for numerical simulations considering cross-diffusive states.

	Figure	τ	β	α	r	k	d_{11}	d_{12}	d_{21}	d_{22}
(22)	Figures 42 and 43	2.316924	0.77	0.76	0.93	1	0.02	0.01	0.01	0.04
(23)	Figures 44 and 45	1.2	0.5	0.4	0.8	1	0.02	0.01	0.01	0.0582753
(24)	Figures 46 and 47	2.316924	0.77	0.76	0.93	1	0.02	0.01	0.01	0.04786
(25)	Figures 48 and 49	2.316924	0.77	0.76	0.93	1	0.02	0.01	0.01	0.048118

(22) With the parameters given by Table 4 (11), we can get $\lambda_1\left(k^2_{l_1,s_1}\right) = 0.759989$, $\lambda_2\left(k^2_{l_1,s_1}\right) = -0.51266$, $P_{\max} = \left|\lambda_2\left(k^2_{l_1,s_1}\right)\right| = 0.759989 < 1$, where systems (2.6) and (2.7) exhibit a stable spatially homogeneous stationary state (Figures 42 and 43).

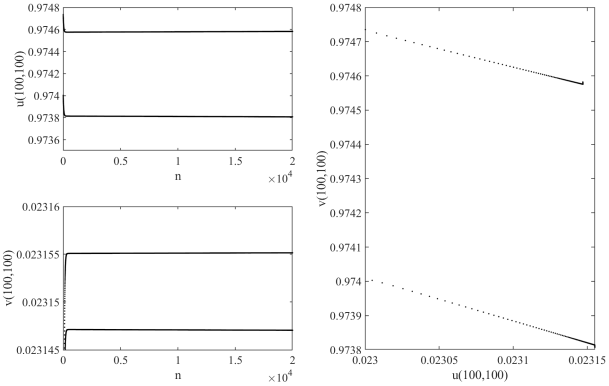

Figure 42. Systems (2.6) and (2.7) undergo a stable spatially homogeneous stationary state for the parameter choices in Table 7 (22).

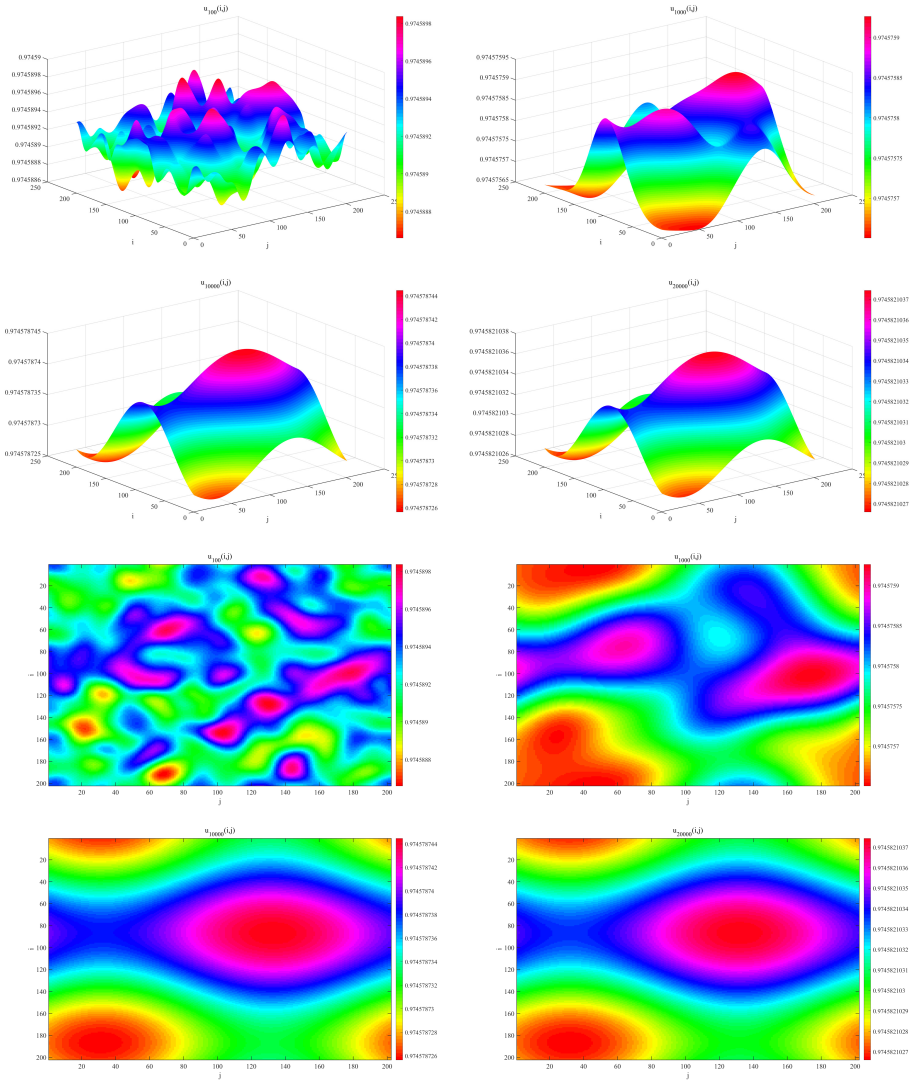

Figure 43. Systems (2.6) and (2.7) undergo a stable spatially homogeneous stationary state.

(23) With the parameters given by Table 4 (12), we can get $\lambda_1\left(k^2_{l_1,s_1}\right) = 0.30886$, $\lambda_2\left(k^2_{l_1,s_1}\right) = -1$, $P_{\max} = \left|\lambda_2\left(k^2_{l_1,s_1}\right)\right| = 1$, where systems (2.6) and (2.7) exhibit Flip bifurcation (Figures 44 and 45).

(24) With the parameters given by Table 4 (13), we can get $\lambda_1\left(k^2_{l_1,s_1}\right) = 0.664292$, $\lambda_2\left(k^2_{l_1,s_1}\right) = -1$, $P_{\max} = \left|\lambda_2\left(k^2_{l_1,s_1}\right)\right| = 1$, where systems (2.6) and (2.7) exhibit a Flip-Flip bifurcation (Figures 46 and 47).

(25) With the parameters given by Table 4 (14), we can get $\lambda_1\left(k^2_{l_2,s_2}\right) = 0.662093$, $\lambda_2\left(k^2_{l_2,s_2}\right) = -1.016646$, $P_{\max} = \left|\lambda_2\left(k^2_{l_2,s_2}\right)\right| = 1.016646 > 1$, where systems (2.6) and (2.7) exhibit Flip-Turing instability (Figures 48 and 49).

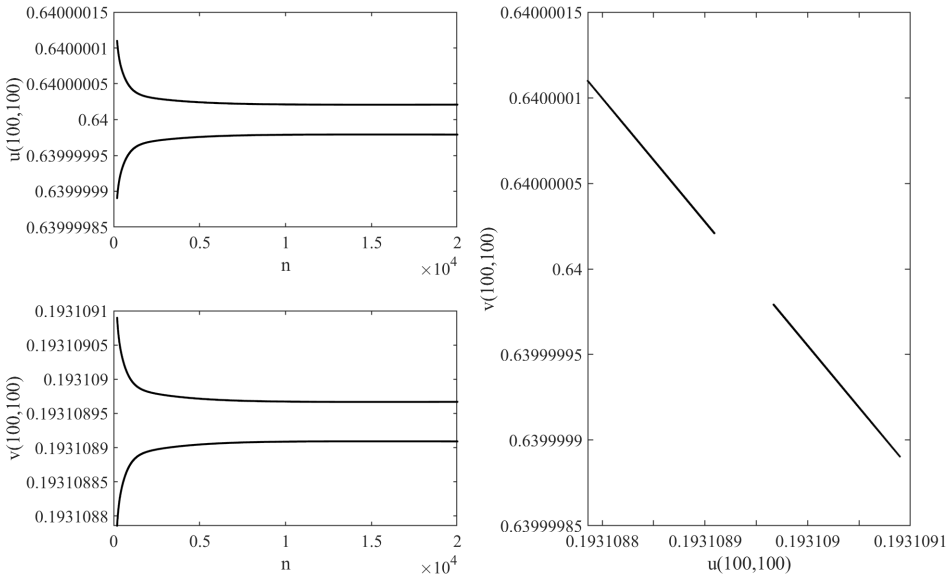

Figure 44. Systems (2.6) and (2.7) undergo a Flip bifurcation for the parameter choices in Table 7 (23).

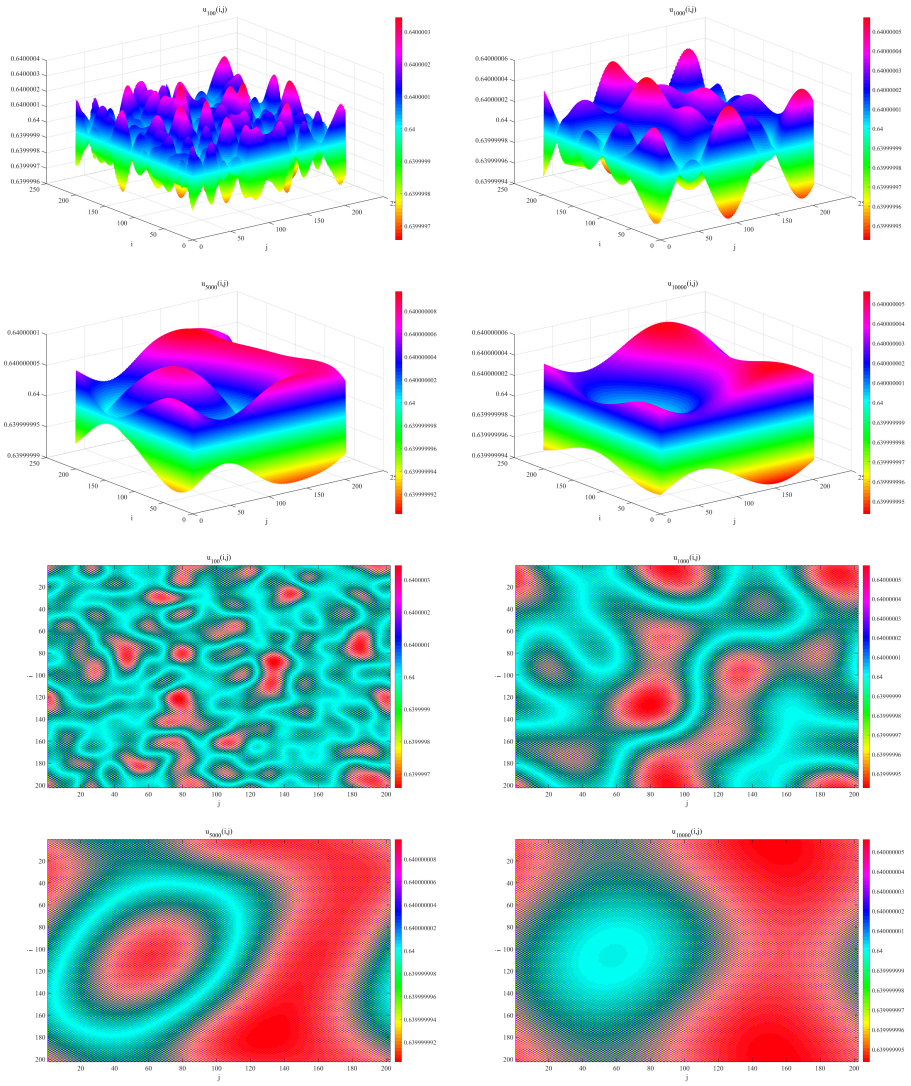

Figure 45. Systems (2.6) and (2.7) undergo a Flip bifurcation.

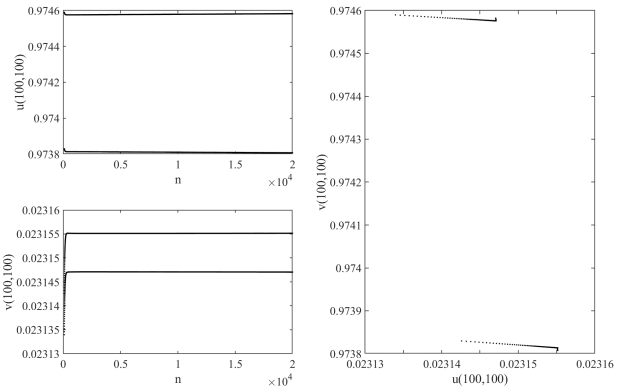

Figure 46. Systems (2.6) and (2.7) undergo a Flip-Flip bifurcation for the parameter choices in Table 7 (24).

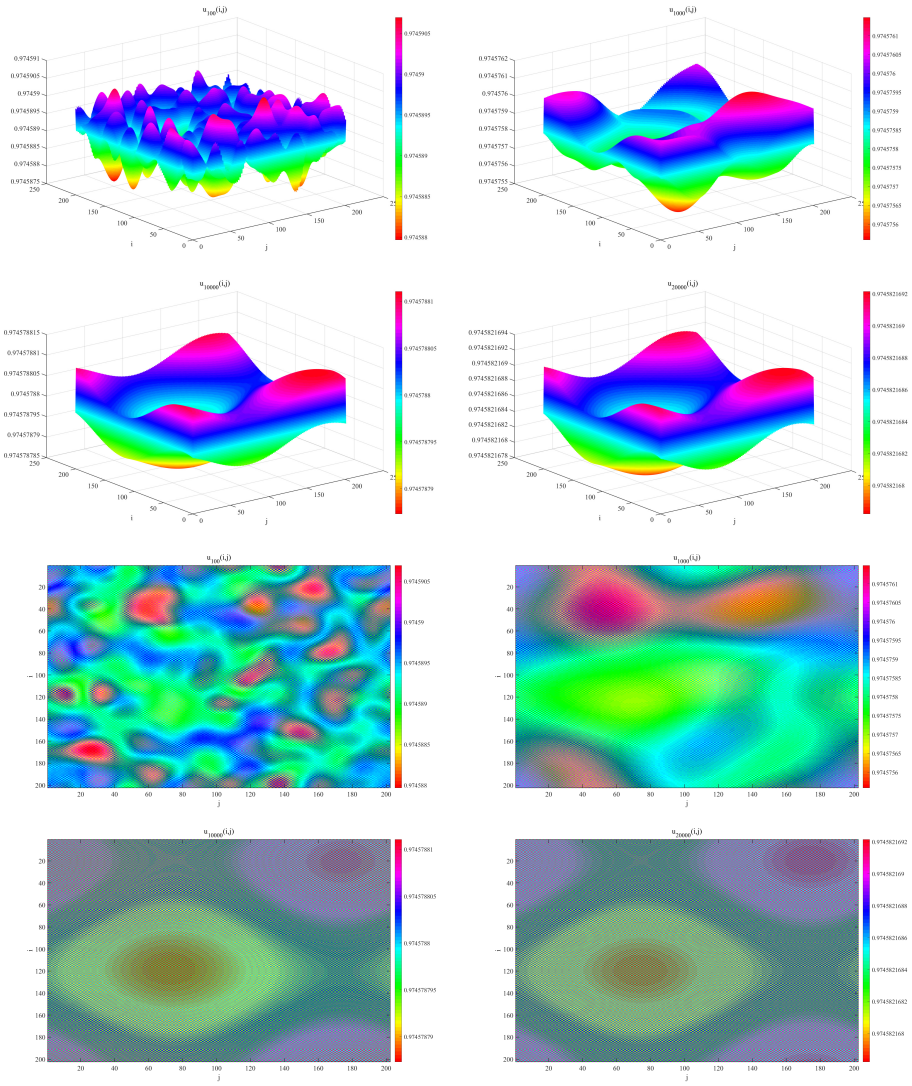

Figure 47. Systems (2.6) and (2.7) undergo a Flip-Flip bifurcation.

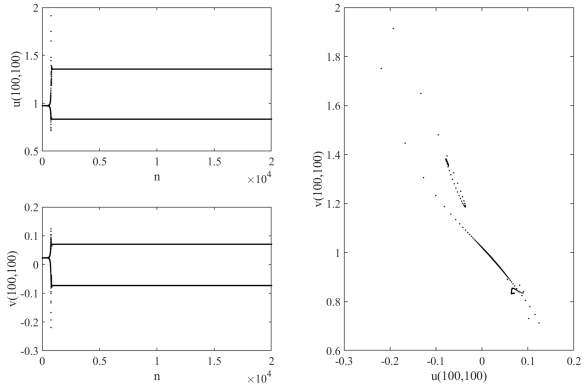

Figure 48. Systems (2.6) and (2.7) undergo Flip-Turing instability for the parameter choices in Table 7 (25).

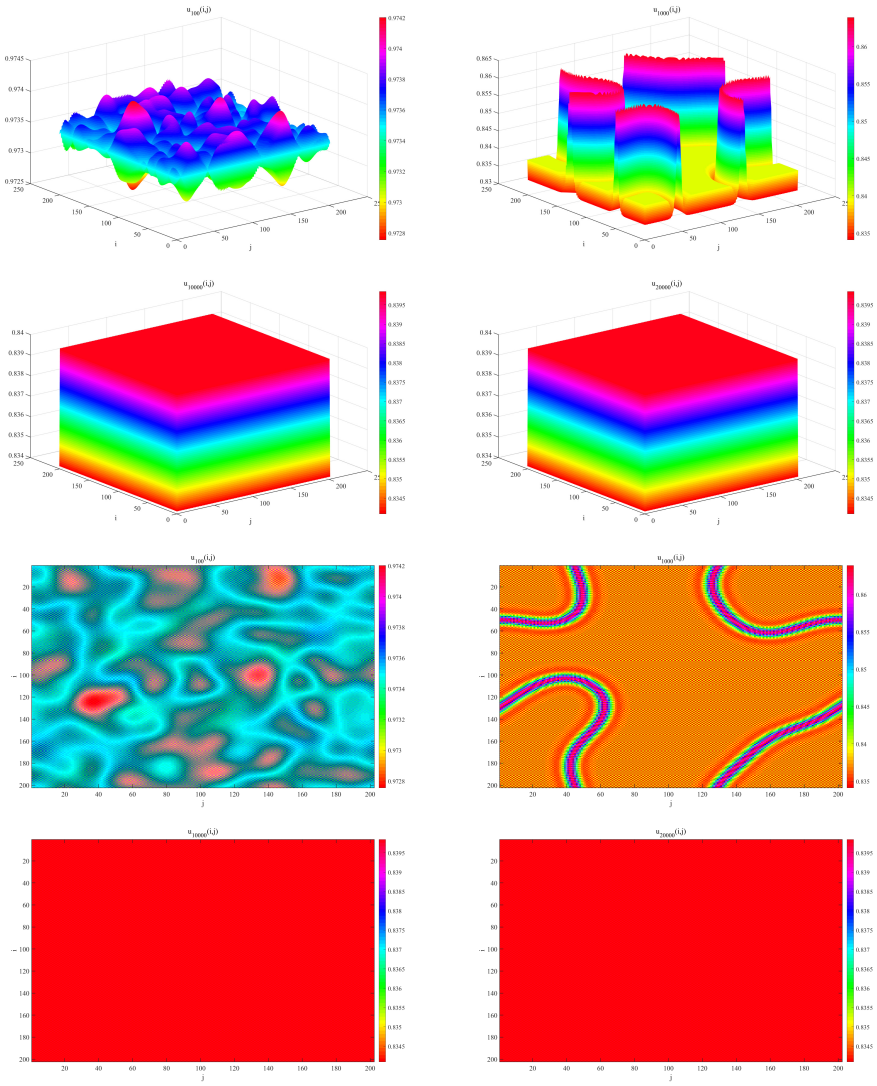

Figure 49. Systems (2.6) and (2.7) undergo Flip-Turing instability.

Remark 5.1. *By adjusting the diffusion coefficient, we simulate different ecological conditions and observe changes in the balance between predators and prey. This study enhances our understanding of how ecosystems maintain stability or undergo changes under varying environmental pressures. An in-depth exploration of the effects of different diffusion coefficients on the predator-prey system provides a crucial theoretical foundation for ecological management and conservation. Managers can regulate ecological balance, promote biodiversity, and effectively prevent overpopulation or extinction of species by controlling the dispersal ability of specific species, thereby maintaining the health of the ecosystem. Studying the phenomenon of bifurcation in the predator-prey system enables us to better predict the future development trends of ecosystems and speculate possible stable or unstable states based on parameter changes, enabling the implementation of appropriate management measures to ensure the stability and sustainability of the ecosystem.*

6. Conclusions

In this paper, we discretize a continuous predator-prey model with diffusion. To better reflect real-world contexts, we adopt a diffusion-followed-by-reaction strategy to optimize the discretized reaction-diffusion model. Given the limited analyses of such discrete predator-prey models with diffusion properties in current research, we adopt a CML modeling approach and introduce a diffusion factor to enhance the accuracy of models. This innovation aims to more accurately model real-world biological scenarios.

In the absence of diffusion, we establish the asymptotic stability conditions, as well as the conditions for the occurrence of the Neimark-Sacker bifurcation and the Flip bifurcation. We complete the computation of the canonical forms of these two bifurcations and present the theorems of Turing instability in different states occurring in spatial inhomogeneity. We then verify the four theorems through numerical simulations. By calculating the maximum Lyapunov exponent and generating bifurcation maps, we illustrate the transition of the system from the bifurcated state to the chaotic state. By adjusting the diffusion coefficients, we observe that the system exhibits different spatial patterns. These simulation results show that the predator-prey model implies extremely complex spatio-temporal dynamic behavior.

The Neimark-Sacker bifurcation vividly illustrates the characteristics of cyclic fluctuations and rhythmic changes in biological populations, phenomena that are prevalent in nature. These fluctuations enable populations to better adapt to environmental changes, thereby effectively maintaining ecological balance. Through Neimark-Sacker bifurcation analysis, we can observe the dynamic behaviors of populations under varying environmental conditions, gaining insights into how they respond to external pressures and resource fluctuations through periodic changes. This adaptive capacity not only aids in the survival and reproduction of populations but also contributes to the stability of ecosystems on a broader scale.

Conversely, the Flip bifurcation uncovers the pattern whereby the period of population size fluctuations increases as system parameters change. This finding indicates that as environmental factors evolve, the dynamic characteristics of populations undergo significant alterations, potentially leading to more intricate ecological interactions and the evolution of population structures. Flip bifurcation analyses serve as a crucial tool for understanding how populations respond to diverse ecological conditions and how regulating relevant parameters can influence their stability and volatility.

Moreover, Turing analysis reveals the complex spatial distribution patterns between predators and prey. This analytical approach enhances our understanding of how different ecological niches are spatially formed and how the interactions between predators and prey impact their distribution and abundance. By studying Turing's model, we can delve deeper into the spatial dynamics within ecosystems, uncovering the underlying mechanisms that govern population distribution.

In summary, bifurcation analysis offers a novel perspective to comprehensively understand the nonlinear dynamics of biological populations. By integrating Neimark-Sacker bifurcation, Flip bifurcation, and Turing analysis, we not only gain a clearer understanding of population dynamics but also establish a scientific foundation for ecological management and conservation efforts. The insights derived from these analyses provide essential theoretical support for exploring the complexity and diversity of ecosystems, thereby enhancing our understanding of ecological balance and sustainable development.

Through these studies, we gain a deeper understanding of the complexity and diversity of the natural world, providing solid scientific support for the protection of the ecological environment and the maintenance of ecological balance.

Author contributions

Wei Li: Conceptualization, Data curation, Formal analysis, Investigation, Methodology, Resources, Software, Visualization, Writing–original draft, Writing–review and editing; Qingkai Xu: Data curation, Formal analysis, Methodology, Software, Writing–review and editing; Xingjian Wang: Funding acquisition, Project administration, Resources, Supervision, Validation, Writing–review and editing; Chunrui Zhang: Conceptualization, Methodology, Project administration, Resources, Supervision, Writing–review and editing. All authors have read and agreed to the published version of the manuscript.

Acknowledgments

This research was supported by the Natural Science Foundation of Heilongjiang Province under Grant Number: LH2020C048.

Use of Generative-AI tools declaration

The authors declare they have not used Artificial Intelligence (AI) tools in the creation of this article.

Conflict of interest

The authors declare that there are no conflicts of interest in this paper.

References

1. S. Motta, F. Pappalardo, Mathematical modeling of biological systems, *Brief. Bioinform.*, **14** (2013), 411–422. https://doi.org/10.1093/bib/bbs061
2. J. B. Johnson, K. S. Omland, Model selection in ecology and evolution, *Trends Ecol. Evol.*, **19** (2004), 101–108. https://doi.org/10.1016/j.tree.2003.10.013
3. Y. Q. Liu, X. Y. Li, Dynamics of a discrete predator-prey model with Holling-II functional response, *Int. J. Biomath.*, **14** (2021), 2150068. https://doi.org/10.1142/S1793524521500686
4. R. Saadeh, A. Abbes, A. Al-Husban, A. Ouannas, G. Grassi, The fractional discrete predator-prey model: chaos, control and synchronization, *Fractal Fract.*, **7** (2023), 120. https://doi.org/10.3390/fractalfract7020120
5. W. Li, C. R. Zhang, M. Wang, Analysis of the dynamical properties of discrete predator-prey systems with fear effects and refuges, *Discrete Dyn. Nat. Soc.*, **2024** (2024), 9185585. https://doi.org/10.1155/2024/9185585

6. S. Ruan, On nonlinear dynamics of predator-prey models with discrete delay, *Math. Model. Nat. Phenom.*, **4** (2009), 140–188. https://doi.org/10.1051/mmnp/20094207
7. R. Ahmed, N. Tahir, N. A. Shah, An analysis of the stability and bifurcation of a discrete-time predator-prey model with the slow-fast effect on the predator, *Chaos*, **34** (2024), 033127. https://doi.org/10.1063/5.0185809
8. T. S. Huang, H. Y. Zhang, X. B. Cong, G. Pan, X. M. Zhang, Z. Liu, Exploring spatiotemporal complexity of a predator-prey system with migration and diffusion by a three-chain coupled map lattice, *Complexity*, **2019** (2019), 3148323. https://doi.org/10.1155/2019/3148323
9. X. T. Zhang, C. R. Zhang, Y. Z. Zhang, Discrete kinetic analysis of a general reaction-diffusion model constructed by Euler discretization and coupled map lattices, *Math. Comput. Simul.*, **225** (2024), 1218–1236. https://doi.org/10.1016/j.matcom.2024.03.028
10. X. T. Zhang, C. R. Zhang, Y. Z. Zhang, Pattern dynamics analysis of a time-space discrete FitzHugh-Nagumo (FHN) model based on coupled map lattices, *Comput. Math. Appl.*, **157** (2024), 92–123. https://doi.org/10.1016/j.camwa.2023.12.030
11. A. J. Lotka, *Elements of physical biology*, Williams and Wilkins, 1925.
12. V. Volterra, Fluctuations in the abundance of a species considered mathematically, *Nature*, **118** (1926), 558–560. https://doi.org/10.1038/118558a0
13. Z. M. He, B. Li, Complex dynamic behavior of a discrete-time predator-prey system of Holling-III type, *Adv. Differ. Equ.*, **2014** (2014), 1–13. https://doi.org/10.1186/1687-1847-2014-180
14. S. G. Mortoja, P. Panja, S. K. Mondal, Dynamics of a predator-prey model with nonlinear incidence rate, Crowley-Martin type functional response and disease in prey population, *Ecol. Genet. Genomics*, **10** (2019), 100035. https://doi.org/10.1016/j.egg.2018.100035
15. D. P. Hu, H. J. Cao, Stability and bifurcation analysis in a predator-prey system with Michaelis-Menten type predator harvesting, *Nonlinear Anal. Real World Appl.*, **33** (2017), 58–82. https://doi.org/10.1016/j.nonrwa.2016.05.010
16. H. I. Freedman, R. M. Mathsen, Persistence in predator-prey systems with ratio-dependent predator influence, *Bull. Math. Biol.*, **55** (1993), 817–827.
17. H. J. Alsakaji, S. Kundu, F. A. Rihan, Delay differential model of one-predator two-prey system with Monod-Haldane and holling type II functional responses, *Appl. Math. Comput.*, **397** (2021), 125919. https://doi.org/10.1016/j.amc.2020.125919
18. V. Ajraldi, M. Pittavino, E. Venturino, Modeling herd behavior in population systems, *Nonlinear Anal. Real World Appl.*, **12** (2011), 2319–2338. https://doi.org/10.1016/j.nonrwa.2011.02.002
19. X. Y. Wang, L. Zanette, X. F. Zou, Modelling the fear effect in predator-prey interactions, *J. Math. Biol.*, **73** (2016), 1179–1204. https://doi.org/10.1007/s00285-016-0989-1
20. H. S. Zhang, Y. L. Cai, S. M. Fu, W. M. Wang, Impact of the fear effect in a prey-predator model incorporating a prey refuge, *Appl. Math. Comput.*, **356** (2019), 328–337. https://doi.org/10.1016/j.amc.2019.03.034
21. H. N. Fakhry, R. K. Naji, The dynamics of a square root prey-predator model with fear, *Iraqi J. Sci.*, **61** (2020), 139–146. https://doi.org/10.24996/ijs.2020.61.1.15

22. J. I. Tello, D. Wrzosek, Predator-prey model with diffusion and indirect prey-taxis, *Math. Models Methods Appl. Sci.*, **26** (2016), 2129–2162. https://doi.org/10.1142/S0218202516400108

23. J. P. Wang, M. X. Wang, The dynamics of a predator-prey model with diffusion and indirect prey-taxis, *J. Dyn. Differ. Equ.*, **32** (2020), 1291–1310. https://doi.org/10.1007/s10884-019-09778-7

24. M. Sambath, K. Balachandran, L. N. Guin, Spatiotemporal patterns in a predator-prey model with cross-diffusion effect, *Int. J. Bifur. Chaos*, **28** (2018), 1830004. https://doi.org/10.1142/S0218127418300045

25. W. M. Wang, Y. Z. Lin, L. Zhang, F. Rao, Y. J. Tan, Complex patterns in a predator-prey model with self and cross-diffusion, *Commun. Nonlinear Sci. Numer. Simul.*, **16** (2011), 2006–2015. https://doi.org/10.1016/j.cnsns.2010.08.035

26. L. N. Guin, Existence of spatial patterns in a predator-prey model with self- and cross-diffusion, *Appl. Math. Comput.*, **226** (2014), 320–335. https://doi.org/10.1016/j.amc.2013.10.005

27. R. Han, L. N. Guin, B. X. Dai, Cross-diffusion-driven pattern formation and selection in a modified Leslie-Gower predator-prey model with fear effect, *J. Biol. Syst.*, **28** (2020), 27–64. https://doi.org/10.1142/S0218339020500023

28. Y. Sun, J. L. Wang, Y. Li, Y. H. Zhu, H. K. Tai, X. Y. Ma, Spatiotemporal complexity analysis of a discrete space-time cancer growth model with self-diffusion and cross-diffusion, *Adv. Contin. Discrete Models*, **28** (2024), 37. https://doi.org/10.1186/s13662-024-03839-y

29. F. X. Mai, L. J. Qin, G. Zhang, Turing instability for a semi-discrete Gierer-Meinhardt system, *Phys. A*, **391** (2012), 2014–2022. https://doi.org/10.1016/j.physa.2011.11.034

30. L. Xu, L. J. Zhao, Z. X. Chang, J. T. Feng, G. Zhang, Turing instability and pattern formation in a semi-discrete Brusselator model, *Modern Phys. Lett. B*, **27** (2013), 1350006. https://doi.org/10.1142/S0217984913500061

31. F. F. Zhang, H. Y. Zhang, T. S. Huang, T. X. Meng, S. N. Ma, Coupled effects of Turing and Neimark-Sacker bifurcations on vegetation pattern self-organization in a discrete vegetation-sand model, *Entropy*, **19** (2017), 478. https://doi.org/10.3390/e19090478

32. A. M. Turing, The chemical basis of morphogenesis, *Bull. Math. Biol.*, **52** (1990), 153–197. https://doi.org/10.1007/BF02459572

33. Y. Zhou, X. P. Yan, C. H. Zhang, Turing patterns induced by self-diffusion in a predator-prey model with schooling behavior in predator and prey, *Nonlinear Dyn.*, **105** (2021), 3731–3747. https://doi.org/10.1007/s11071-021-06743-2

34. T. H. Li, X. T. Zhang, C. R. Zhang, Pattern dynamics analysis of a space-time discrete spruce budworm model, *Chaos Solitons Fract.*, **179** (2024), 114423. https://doi.org/10.1016/j.chaos.2023.114423

35. X. T. Zhang, C. R. Zhang, The diffusion-driven instability for a general time-space discrete host-parasitoid model, *Discrete Dyn. Nat. Soc.*, **2023** (2023), 7710701. https://doi.org/10.1155/2023/7710701

36. S. Djilali, Spatiotemporal patterns induced by cross-diffusion in predator-prey model with prey herd shape effect, *Int. J. Biomath.*, **13** (2020), 2050030. https://doi.org/10.1142/s1793524520500308

37. Z. M. Bi, S. T. Liu, M. Ouyang, Three-dimensional pattern dynamics of a fractional predator-prey model with cross-diffusion and herd behavior, *Appl. Math. Comput.*, **412** (2022), 126955. https://doi.org/10.1016/j.amc.2022.126955

38. R. J. Han, L. N. Guin, S. Acharya, Complex dynamics in a reaction-cross-diffusion model with refuge depending on predator-prey encounters, *Eur. Phys. J. Plus*, **137** (2022), 134. https://doi.org/10.1140/epjp/s13360-022-02358-7

39. F. Souna, S. Djilali, A. Lakmeche, Spatiotemporal behavior in a predator-prey model with herd behavior and cross-diffusion and fear effect, *Eur. Phys. J. Plus*, **136** (2021), 474. https://doi.org/10.1140/epjp/s13360-021-01489-7

40. E. Tulumello, M. C. Lombardo, M. Sammartino, Cross-diffusion driven instability in a predator-prey system with cross-diffusion, *Acta Appl. Math.*, **132** (2014), 621–633. https://doi.org/10.1007/s10440-014-9935-7

41. S. Ghorai, S. Poria, Turing patterns induced by cross-diffusion in a predator-prey system in presence of habitat complexity, *Chaos Solitons Fract.*, **91** (2016), 421–429. https://doi.org/10.1016/j.chaos.2016.07.003

42. H. L. Yuan, J. H. Wu, Y. F. Jia, H. Nie, Coexistence states of a predator-prey model with cross-diffusion, *Nonlinear Anal. Real World Appl.*, **41** (2018), 179–203. https://doi.org/10.1016/j.nonrwa.2017.10.009

43. X. S. Tang, Y. L. Song, T. H. Zhang, Turing-Hopf bifurcation analysis of a predator-prey model with herd behavior and cross-diffusion, *Nonlinear Dyn.*, **86** (2016), 73–89. https://doi.org/10.1007/s11071-016-2873-3

44. J. Guckenheimer, P. Holmes, *Nonlinear oscillations, dynamical systems, and bifurcations of vector fields*, New York: Springer, 1983. https://doi.org/10.1007/978-1-4612-1140-2

45. L. Bai, G. Zhang, Nontrivial solutions for a nonlinear discrete elliptic equation with periodic boundary conditions, *Appl. Math. Comput.*, **210** (2009), 321–333. https://doi.org/10.1016/j.amc.2008.12.024

Appendix

Appendix A

$$\xi_{20} = \frac{1}{8}\left(\left(f_{12_{U_{1,n}U_{1,n}}} - f_{12_{V_{1,n}V_{1,n}}} + 2g_{12_{U_{1,n}V_{1,n}}}\right) + i\left(g_{12_{U_{1,n}U_{1,n}}} - g_{12_{V_{1,n}V_{1,n}}} - 2f_{12_{U_{1,n}V_{1,n}}}\right)\right),$$

$$\xi_{11} = \frac{1}{4}\left(f_{12_{U_{1,n}U_{1,n}}} + f_{12_{V_{1,n}V_{1,n}}} + i\left(g_{12_{U_{1,n}U_{1,n}}} + g_{12_{V_{1,n}V_{1,n}}}\right)\right),$$

$$\xi_{02} = \frac{1}{8}\left(f_{12_{U_{1,n}U_{1,n}}} - f_{12_{V_{1,n}V_{1,n}}} - 2g_{12_{U_{1,n}V_{1,n}}} + i\left(g_{12_{U_{1,n}U_{1,n}}} - g_{12_{V_{1,n}V_{1,n}}} + 2f_{12_{U_{1,n}V_{1,n}}}\right)\right),$$

$$\xi_{21} = \frac{1}{16}\left(f_{12_{U_{1,n}U_{1,n}U_{1,n}}} + f_{12_{U_{1,n}V_{1,n}V_{1,n}}} + g_{12_{U_{1,n}U_{1,n}V_{1,n}}} + g_{12_{V_{1,n}V_{1,n}V_{1,n}}} + i\left(g_{12_{U_{1,n}U_{1,n}U_{1,n}}} + g_{12_{U_{1,n}V_{1,n}V_{1,n}}}\right.\right.$$
$$\left.\left. - f_{12_{U_{1,n}U_{1,n}V_{1,n}}} - f_{12_{V_{1,n}V_{1,n}V_{1,n}}}\right)\right),$$

$$f_{12_{U_{1,n}U_{1,n}}}=\left.\frac{\partial^2 f_{12}\left(U_{1,n},V_{1,n}\right)}{\partial\left(U_{1,n}\right)^2}\right|_{U_{1,n}=V_{1,n}=0},\quad g_{12_{U_{1,n}U_{1,n}}}=\left.\frac{\partial^2 f_{12}\left(U_{1,n},V_{1,n}\right)}{\partial\left(U_{1,n}\right)^2}\right|_{U_{1,n}=V_{1,n}=0},$$

$$f_{12_{U_{1,n}V_{1,n}}}=\left.\frac{\partial^2 f_{12}\left(U_{1,n},V_{1,n}\right)}{\partial U_{1,n}V_{1,n}}\right|_{U_{1,n}=V_{1,n}=0},\quad g_{12_{U_{1,n}V_{1,n}}}=\left.\frac{\partial^2 f_{12}\left(U_{1,n},V_{1,n}\right)}{\partial U_{1,n}V_{1,n}}\right|_{U_{1,n}=V_{1,n}=0},$$

$$f_{12_{V_{1,n}V_{1,n}}}=\left.\frac{\partial^2 f_{12}\left(U_{1,n},V_{1,n}\right)}{\partial\left(V_{1,n}\right)^2}\right|_{U_{1,n}=V_{1,n}=0},\quad g_{12_{V_{1,n}V_{1,n}}}=\left.\frac{\partial^2 f_{12}\left(U_{1,n},V_{1,n}\right)}{\partial\left(V_{1,n}\right)^2}\right|_{U_{1,n}=V_{1,n}=0},$$

$$f_{12_{U_{1,n}U_{1,n}U_{1,n}}}=\left.\frac{\partial^3 f_{12}\left(U_{1,n},V_{1,n}\right)}{\partial\left(U_{1,n}\right)^3}\right|_{U_{1,n}=V_{1,n}=0},\quad g_{12_{U_{1,n}U_{1,n}U_{1,n}}}=\left.\frac{\partial^3 f_{12}\left(U_{1,n},V_{1,n}\right)}{\partial\left(U_{1,n}\right)^3}\right|_{U_{1,n}=V_{1,n}=0},$$

$$f_{12_{U_{1,n}U_{1,n}V_{1,n}}}=\left.\frac{\partial^3 f_{12}\left(U_{1,n},V_{1,n}\right)}{\partial\left(U_{1,n}\right)^2\partial V_{1,n}}\right|_{U_{1,n}=V_{1,n}=0},\quad g_{12_{U_{1,n}U_{1,n}V_{1,n}}}=\left.\frac{\partial^3 f_{12}\left(U_{1,n},V_{1,n}\right)}{\partial\left(U_{1,n}\right)^2\partial V_{1,n}}\right|_{U_{1,n}=V_{1,n}=0},$$

$$g_{12_{U_{1,n}V_{1,n}V_{1,n}}}=\left.\frac{\partial^3 f_{12}\left(U_{1,n},V_{1,n}\right)}{\partial U_{1,n}\partial\left(V_{1,n}\right)^2}\right|_{U_{1,n}=V_{1,n}=0},\quad f_{12U_{1,n}V_{1,n}V_{1,n}}=\left.\frac{\partial^3 f_{12}\left(U_{1,n},V_{1,n}\right)}{\partial U_{1,n}\partial\left(V_{1,n}\right)^2}\right|_{U_{1,n}=V_{1,n}=0},$$

$$f_{12_{V_{1,n}V_{1,n}V_{1,n}}}=\left.\frac{\partial^3 f_{12}\left(U_{1,n},V_{1,n}\right)}{\partial\left(V_{1,n}\right)^3}\right|_{U_{1,n}=V_{1,n}=0},\quad g_{12_{V_{1,n}V_{1,n}V_{1,n}}}=\left.\frac{\partial^3 f_{12}\left(U_{1,n},V_{1,n}\right)}{\partial\left(V_{1,n}\right)^3}\right|_{U_{1,n}=V_{1,n}=0}.$$

Appendix B

$$\begin{aligned}f_{21}\left(u_{2,n},v_{2,n},\widetilde{\tau}\right)=&a_{200}(u_{2,n})^2+a_{110}u_{2,n}v_{2,n}+a_{101}u_{2,n}\widetilde{\tau}+a_{020}(v_{2,n})^2+a_{011}v_{2,n}\widetilde{\tau}+a_{002}(\widetilde{\tau})^2\\&+a_{300}(u_{2,n})^3+a_{210}(u_{2,n})^2v_{2,n}+a_{201}(u_{2,n})^2\widetilde{\tau}+a_{120}u_{2,n}(v_{2,n})^2+a_{030}(v_{2,n})^3\\&+a_{021}(v_{2,n})^2\widetilde{\tau}+a_{102}u_{2,n}(\widetilde{\tau})^2+a_{012}v_{2,n}(\widetilde{\tau})^2+a_{003}(\widetilde{\tau})^3+a_{111}u_{2,n}v_{2,n}\widetilde{\tau},\end{aligned}$$

$$\begin{aligned}g_{21}\left(u_{2,n},v_{2,n},\widetilde{\tau}\right)=&b_{200}(u_{2,n})^2+b_{110}u_{2,n}v_{2,n}+b_{101}u_{2,n}\widetilde{\tau}+b_{020}(v_{2,n})^2+b_{011}v_{2,n}\widetilde{\tau}+b_{002}(\widetilde{\tau})^2\\&+b_{300}(u_{2,n})^3+b_{210}(u_{2,n})^2v_{2,n}+b_{201}(u_{2,n})^2\widetilde{\tau}+b_{120}u_{2,n}(v_{2,n})^2+b_{030}(v_{2,n})^3\\&+b_{021}(v_{2,n})^2\widetilde{\tau}+b_{102}u_{2,n}(\widetilde{\tau})^2+b_{012}v_{2,n}(\widetilde{\tau})^2+b_{003}(\widetilde{\tau})^3+b_{111}u_{2,n}v_{2,n}\widetilde{\tau},\end{aligned}$$

$$a_{100}=1-\frac{v^*\tau_2^*}{2\sqrt{u^*}}+\frac{r\left(1-2u^*\right)\tau_2^*}{1+kv^*},\ a_{010}=-\sqrt{u^*}\tau_2^*+\frac{kr\left(-1+u^*\right)u^*\tau_2^*}{\left(1+kv^*\right)^2},$$

$$a_{001}=-\sqrt{u^*}v^*-\frac{r\left(-1+u^*\right)u^*}{1+kv^*},\ a_{200}=\frac{v^*\tau_2^*}{8(u^*)^{3/2}}-\frac{r\tau_2^*}{1+kv^*},\ a_{110}=-\frac{\tau_2^*}{2\sqrt{u^*}}+\frac{kr\left(-1+2u^*\right)\tau_2^*}{\left(1+kv^*\right)^2},$$

$$a_{101}=-\frac{v^*}{2\sqrt{u^*}}+\frac{r\left(1-2u^*\right)}{1+kv^*},\ a_{011}=-\sqrt{u^*}+\frac{kr\left(-1+u^*\right)u^*}{\left(1+kv^*\right)^2},\ a_{300}=-\frac{v^*\tau_2^*}{16(u^*)^{5/2}},$$

$$a_{210}=\frac{\tau_2^*}{8(u^*)^{3/2}}+\frac{kr\tau_2^*}{\left(1+kv^*\right)^2},\ a_{201}=\frac{v^*}{8(u^*)^{3/2}}-\frac{r}{1+kv^*},\ a_{111}=-\frac{1}{2\sqrt{u^*}}+\frac{kr\left(-1+2u^*\right)}{\left(1+kv^*\right)^2},$$

$$a_{020}=-\frac{k^2r\left(-1+u^*\right)u^*\tau_2^*}{\left(1+kv^*\right)^3},\ a_{120}=\frac{k^2r\left(1-2u^*\right)\tau_2^*}{\left(1+kv^*\right)^3},\ a_{030}=\frac{k^3r\left(-1+u^*\right)u^*\tau_2^*}{\left(1+kv^*\right)^4},$$

$$a_{021}=-\frac{k^2r\left(-1+u^*\right)u^*}{\left(1+kv^*\right)^3},\ a_{002}=a_{102}=a_{012}=a_{003}=0,$$

$$b_{100}=\frac{\beta v^*\tau_2^*}{2\sqrt{u^*}},\ b_{010}=1-\alpha\tau_2^*+\beta\sqrt{u^*}\tau_2^*,\ b_{001}=-\alpha v^*+\beta\sqrt{u^*}v^*,\ b_{200}=-\frac{\beta v^*\tau_2^*}{8(u^*)^{3/2}},$$

$$b_{110} = \frac{\beta\tau_2^*}{2\sqrt{u^*}},\ b_{101} = \frac{\beta v^*}{2\sqrt{u^*}},\ b_{011} = -\alpha + \beta\sqrt{u^*},\ b_{300} = \frac{\beta v^*\tau_2^*}{16(u^*)^{5/2}},\ b_{210} = -\frac{\beta\tau_2^*}{8(u^*)^{3/2}},$$

$$b_{201} = -\frac{\beta}{8(u^*)^{3/2}},\ b_{111} = \frac{\beta}{2\sqrt{u^*}},\ b_{002} = b_{020} = b_{120} = b_{030} = b_{021} = b_{102} = b_{012} = b_{003} = 0.$$